Effect of Sintering Additives (V_2O_5, B_2O_3, Bi_2O_3) on the Electrical Properties of substituted Y-type Hexagonal Ferrite, $Ba_2Co_{0.6}Cu_{0.4}Zn_{1.0}Fe_{12}O_{22}$

SUBMITTED BY:

Sujit Kumar Giri

711CR1171

UNDER THE SUPERVISION OF:

Prof. J. Bera

IN PARTIAL FULFILLMENT FOR THE AWARD OF THE DEGREE OF

MASTER OF TECHNOLOGY (DUAL DEGREE)

IN CERAMIC ENGINEERING

Department of Ceramic Engineering
National Institute of Technology, Rourkela

2016

NATIONAL INSTITUTE OF TECHNOLOGY
ROURKELA

Supervisor's Certificate

This is to certify that the work presented in the dissertation entitled, "***Effect of Sintering Additives (V_2O_5, Bi_2O_3, B_2O_3) on the Electrical Properties of Co_2-Y Hexagonal Ferrite, $Ba_2Co_{0.6}Cu_{0.4}Zn_{1.0}Fe_{12}O_{22}$*** **"** submitted by **Mr. Sujit Kumar Giri, Roll Number - 711CR1171** is a record of original research carried out by him under my guidance and supervision in partial fulfilment for the requirements of the award of **Master of Technology Dual-Degree** in **Department of Ceramic Engineering.**

To the best of my knowledge, the matter embodied in the thesis has not been submitted to any other university/institute for the award of any Degree/Diploma.

Date: May 31, 2016

Place: Rourkela

Prof. Japes Bera
Department of Ceramic Engineering
National Institute of Technology
Rourkela-769008, Odisha

ACKNOWLEDGEMENT

I wish to express my sincere gratitude to my advisor Prof. Japes Bera, for his inspiring supervision, guidance, encouragement, constructive criticism, and support during the course of this thesis and also in the experimental study of this research work. I would also like to thank him for his constant assistance and encouragement to complete this research work.

I must thank all my professors whose enormous knowledge in the field of hexaferrite has enlightened me in various areas of my project work. Arvind Sir, Bapi *da* and all other staff members of the Ceramic Engineering Department are worth a mention for their timely help which aided to conclude this work within deadline.

I am also obliged to Mr. Vinay Kumar R and all the other research scholars in the Dept. of Ceramic Engineering for their excellent help and support.

Last but not the least, I thank my parents for their unconditional love, constant encouragement, support and faith in me.

Thank you, everyone.

Date: May 31, 2016 Sujit Kumar Giri

Place: Rourkela 711CR1171

ABSTRACT

The effects of B_2O_3, Bi_2O_3 and V_2O_5 sintering additives on sintering temperature, phase stability, microstructure and electromagnetic properties of Cu–Zn co-substituted Co_2-Y ferrite ($Ba_2Co_{0.6}Cu_{0.4}Zn_{1.0}Fe_{12}O_{22}$) was investigated. The ferrite was synthesized by solid oxide route. The XRD result confirms the formation of pure phase at 1000^{o}C. Ferrite with Bi_2O_3 additives showed better shrinkage and densification at 900°C, than B_2O_3 and V_2O_5; V_2O_5 additive had very little effect (less than 5%) on the sintering behavior when sintered at 900^{o}C. However, the ferrite phase decomposed with an addition of 6 wt% V_2O_5, when fired at 1100^{o}C . The higher sintering rate and lower sintering temperature was found in B_2O_3 and Bi_2O_3 added ferrites. There was very little densification in the case of undoped and V_2O_5 doped specimen when sintered at 900°C, while denser microstructure and increased grain growth were observed in the case of the higher B_2O_3 and Bi_2O_3 wt %-content samples.

LIST OF FIGURES

CONTENTS

Chapter 1

INTRODUCTION

Introduction:

1.1. Hexagonal ferrites & their Applications

Developments in the recent years have resulted in technological advancements in communication sector, especially the devices for signal processing has caught everyone's vision. The hexagonal ferrites operating at higher frequenies have made it possible for the shifting of operating frequencies of the devices to higher ranges [1]. The demand of the hexagonal ferrites, referred to as hexaferrites as well, has reached an exponential growth rate since their discovery. The hexaferrites have become so important materials with time finding a magnitude of application areas & accounts for bulk of the global manufacturing of whole magnetic materials. Being components in the electrical devices is one of the common application areas of these ferrites, particularly those which operate at GHz frequencies. Due to their hexagonal crystal structures, the hexaferrites are called so. The general composition BaO-MeO-Fe_2O_3 has numbers of hexagonal ferrite compounds, where Me is a small 2+ ion.

Important types of hexa-ferrites are designated as M, W, Y, Z, X and U types. The chemical formulae of them are:

- Y-type: $Ba_2Me_2Fe_{12}O_{22}$
- M-type: $BaFe_{12}O_{19}$ (BaM) or $SrFe_{12}O_{19}$ (SrM)
- W-type: $BaMe_2Fe_{16}O_{27}$
- Z-type: $Ba_3Me_2Fe_{24}O_{41}$
- X-type: $Ba_2Me_2Fe_{28}O_{46}$
- U-type: $Ba_4Me_2Fe_{36}O_{60}$

All of the hexagonal ferrites have a closely related, highly complex crystal structures. At a simple level, they can all be seen as molecular combinations of the three ferrite compounds: S (spinel, $MeFe_2O_4$), M ($BaFe_{12}O_{19}$) and Y ($Ba_2Me_2Fe_{12}O_{22}$).

The hexagonal ferrites (or hexaferrites) are ferromagnetic materials and their properties are intrinsically linked to their crystalline structures. They all have a magnetocrystalline anisotropy (MCA) i.e., the indced magnetization has a preferred orientation within the crystal structure:

- Easy axis of magnetisation, the **uniaxial** hexaferrites and
- Easy plane (or cone) of magnetisation, known as **hexaplana** ferrites.

All of these compounds are found to have a hexagonal crystal structure, with two crystalline lattice parameters: a, the width of the hexagonal plane, and c, the height of the crystalline lattice. All of them show a preferred direction of magnetization when placed in a magnetic field, giving them an MCA. Y-type is hexaplana ferrites whereas M-, Z-, W-, X- and U-types ferrites are uniaxial. However, Co_2Z, Co_2W, Co_2X and Co_2U ferrites have planar anisotropy [2].

Magnets are used in a multitude of applications, for example motors, generators, transformers, actuators and sensors, information storage, mobile communications, transport, security, defence and aerospace, diagnostic devices and to focus electron beams. The most used magnetic materials are ferromagnetic metals and alloys or ferrimagnetic ceramics. Of the ceramics, by far the most used are hexagonal ferrites, and some of their multitudes of applications are shown in Fig. 1.1.

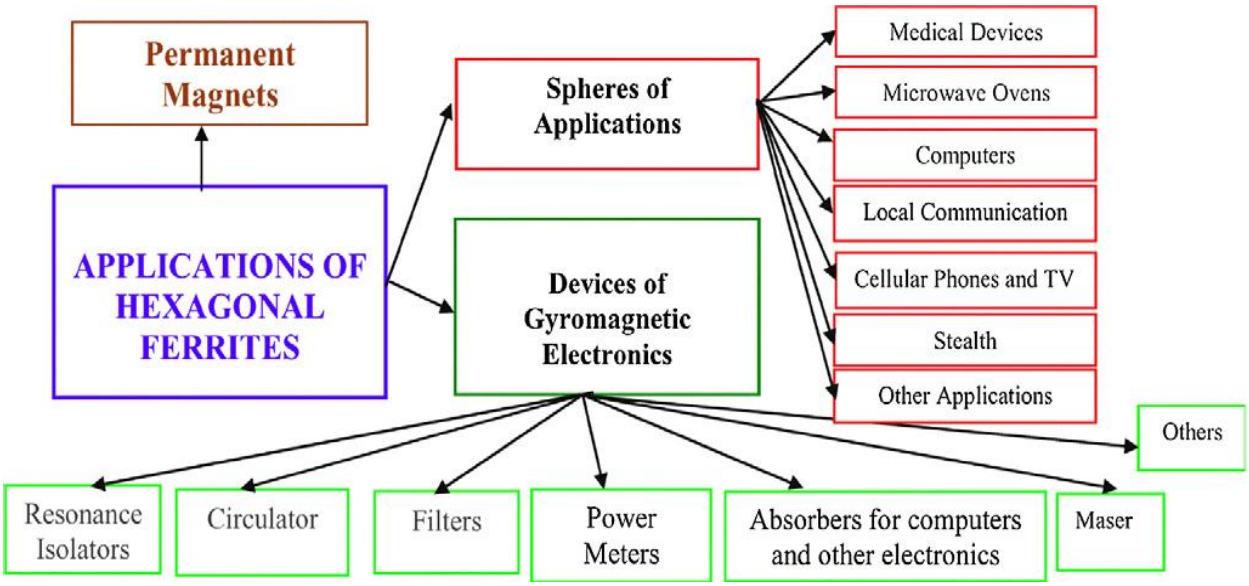

Fig. 1.1. Various application areas of hexaferrites.

The major applications of the hexaferrites has been in the following areas:

- Permanent magnets
- Electrical and Microwave devices
- Data storage and recording
- Plastoferrites
- RAM and microwave/EM wave absorption
- Magnetoelectric (ME) and multiferroic (MF) applications.

In addition to the high operating frequency, current generation electronic devices are becoming smaller with less weight and more efficient day by day. For that, the passive components are used in the form of multilayer chip component and are surface mounted on printed circuit boards. The recent trend is the integration of different passive components onto a single Si-wafer platform enabling more reduction of device volume and weight. For both the technologies, low temperature co-fired ceramics (LTCC) is required for co-sintering with internal metal electrode. One of such component is multilayer ferrite chip inductor (MLFCI) shown in Fig.1.2.

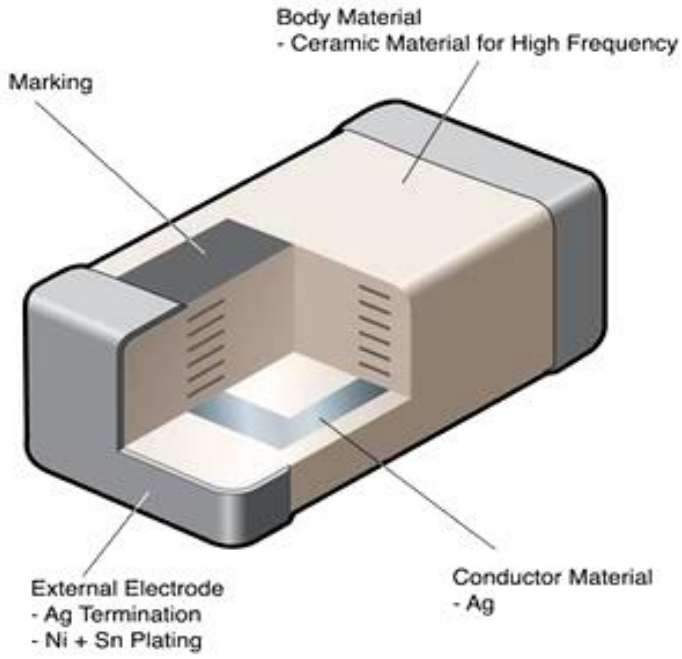

Fig. 1.2. Multilayer ferrite chip inductor.

For the fabrication of MLFCI, ferrite is co-sintered with an internal metal. Silver (Ag) is usually most suitable internal electrode as it has;

- High conductivity
- Lower cost
- Lower electrical losses

1.2. Y-Hexagonal ferrites & the crystal structure

The Y-ferrites were the first ferroxplana ferrites to be discovered, and it is now known that nearly all y-ferrites have a preferred plane of magnetization perpendicular to the c-axis at room temperature. The formula of the Y-ferrites is $Ba_2Me_2Fe_{12}O_{22}$, where Me is a small divalent cation, and the first two to be made were Zn_2Y and Co_2Y. Co_2Y has a planar magnetic anisotropy at room temperature, but these changes to a cone of magnetization below -58 ^oC. From this temperature to the Curie point, the anisotropy remains in the preferred plane. Cu_2Y is the only Y-hexaferrite that has been found to have a preferred uniaxial direction of magnetization.

Structure:

From the crystallographic point of view, the Y-structure can be considered as a stacking of two S-$[Me_2Fe_4O_8]$ and T-$[Ba_2Fe_8O_{14}]$ building blocks along the c-axis. The S-block consists of two oxygen layers and the T-block has four layers with two of them containing Ba.

The molecular unit of Y ferrite is one S and one T unit, with a total of six layers, the unit cell consists of three of these units, with the length of the c-axis being 43.56 Å, and is a member of the space group R_3m (No. 166) [3]. The T block does not have a mirror plane, and therefore a series of three T blocks is required to accommodate the overlap of hexagonal and cubic close packed layers, with the relative positions of the barium atoms repeating every three T blocks. This gives the unit cell formula as simply 3(ST), and the structure is shown in Fig. 1.3.

The Y-ferrites all have lower magnetisation than the M ferrites, the highest being for Zn, Ms=72Am^2kg^{-1} at 0 K) [1], and getting lower in the sequence Zn > Mn > Co > Ni [5]. At room temperature, Zn_2-Y has Ms=42$Am^2\,kg^{-1}$, but the curie point of Zn_2-Y is only 130^o C, and it has a low crystalline anisotropy of only 716 kA m^{-1} (9 kOe) [1]. Ni_2-Y made by Sudakar et al. at only 950 ^oC was a very soft ferrite, with M_s = 25.5 A $m^2\,kg^{-1}$, Hc=16 kA m^{-1} and a T_c of 387 ^oC [6], and it has a higher H_A of 1100 kA m^{-1} (14 kOe) [1]. Co_2-Y has the highest MCA of any hexagonal ferrite, uniaxial or ferroxplana, with a (K1 + 2K2) value of -2.6x10^5 J m^{-3}, K_3= 80 J m^{-3} and the crystalline anisotropy reported originally as H_A=2228 kA m^{-1} (28 kOe) in the preferred plane & only 119 kA m^{-1} in the c-axis, all at room temperature [1].

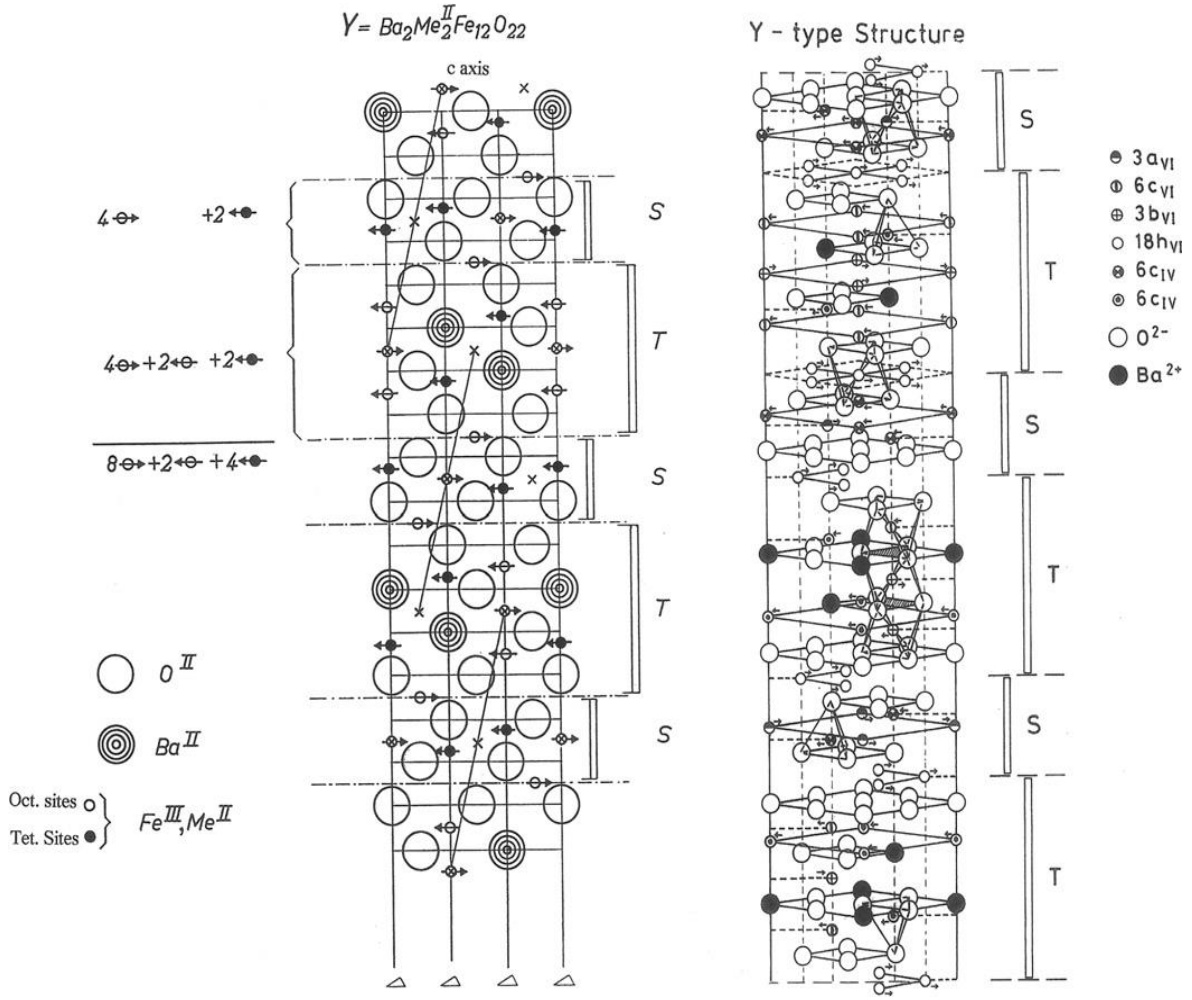

Fig. 1.3. Left: Cross section view of the Y ferrite ($Ba_2Me_2Fe_{12}O_{22}$) structure in which the vertical lines are axes of threefold symmetry [1]. The arrows indicate the orientations of the magnetic moments of the cations relative to the c-axis. Right: Perspective view of the Y structure [4].

Co_2-Y has a moment of 9.8l μ_B, the room temperature saturation magnetisation is 34 A m^2 kg^{-1} and the coercivity is small, with a relatively high Curie point of 340 ^oC [1]. Because of this large negative anisotropy, from T_c to RT and below Co_2Y has an easy plane of magnetisation at 90^o to the c-axis, with H_A peaking at around RT. The Y ferrites may have larger negative K values because there is no five-coordinate site in the T block, and therefore there is a lower spin–orbit coupling contribution to K [7]. The Co^{2+} ions are all in octahedral positions, with the spin orientations 1.1 spin-up & 0.9 spin-down [8]. There is a huge decrease in the anisotropy of Co_2Y to almost $H_A = 0$ at 215 K, below which temperature the ($K_1 + 2 K_2$) anisotropy becomes positive as the easy plane becomes a cone of magnetisation, the angle to the c-axis decreasing from 90^o at 215 K to <70^o at 77 K, with a K_3 value of 200 J m^{-3} at

that temperature [1]. This cone is enough to induce a spontaneous magnetisation along the c-axis at low temperatures, making Co_2Y a hard magnet with a high M_r at 77 K. More recently sintered ceramic Co_2Y has been reported by Obol and Vittoria as having H_A= 2944 kA m^{-1}, a volume magnetisation of 183 kA m^{-1}, and H_c=4.4 kA m^{-1}, which was increased further to H_A= 3342 kA m^{-1} and Hc= 5.3 kA m^{-1} in oriented samples [9]. Randomly oriented polycrystalline Co_2Y fibres sintered at 1000 ^oC/3h had M_s =32.8 A m^2 kg^{-1}, M_r =9.2 A m^2 kg^{-1} and H_c=30 kA m^{-1} [10], and Co_2Y made from an EDTA complex had M_s =28.8-33.4 A m^2 kg^{-1}, and H_c=15-6.7 kA m^{-1}[11]. 180^o domain walls were first demonstrated in Zn_2Y [12], and since then Co_2Y has also been shown to contain stacked layers of domains of equal width separated by 180^o walls, giving the domains a rectangular and not a hexagonal shape [13]. A single domain crystal has also been seen to become split by a 180^o domain wall as the magnetization drops below M_s [14].

Sr_2Zn_2Y showed a strange, non-collinear magnetic structuring due to the Sr^{2+} ion distorting the lattice [15], and therefore the replacement of barium with strontium in Y ferrites steadily reduced the permeability, but a 50% substitution of lead increased it dramatically [16]. In substitutions of Co with Zn to give the compound $Co_{1-x}Zn_xY$ fired at 1000 ^oC/10 h, T_c falls linearly from 340 ^oC (x = 0) to 100 ^oC (x = 1). The M_s values increased with addition, but they were lower than expected with M_s = 26.6 (instead of 34) and 32.9 (instead of 42) A m^2 kg^{-1} for x = 0 and 1 respectively [17]. Zinc weakens the super interactions and lowers T_c, but there is no change in the spin directions so the net magnetic moment increases with addition.

Y-type hexaferrites with planar magneto-crystalline anisotropy has ultrahigh cut-off frequency upto few GHz and excellent magnetic properties in hyper-frequency range. So, it is regarded as the most suitable material in corresponding inductive devices and components. The technology of low temperature co-fired ceramics for surface moulded multi-layer chip components needs the ferrites to be sintered well under 900 ^oC to avoid the melting and diffusion of Ag inner electrode during the co-firing process.

As silver melts at 961 ^oC, the ferrite composition must be co-sintered at a temperature sufficiently lower than that, preferably at 900 ^oC, to prevent possible diffusion of Ag into the ferrite. Otherwise the diffusion of Ag metal may decrease the permeability of the ferrite. For low temperature sintering of the ferrites, usually sintering additives like glass, Bi_2O_3, are used.

However, the sintering additive decreases the permeability of ferrite, and the quantity of additive should be as low as possible. Additionally, sinter-active fine ferrite powders are used for chip fabrication. Another solution could be a suitable modification of the ferrite composition enabling its low temperature sintering.

Various designs for sensors incorporating ferrites have been proposed, including a humidity sensor based upon the change of resistance in a copper–zinc ferrite [18]. Hexaferrites can also find medical applications, for example as components in nuclear magnetic resonance imaging and magnetomotive biomedical implants, but the toxicity of some of the component elements, particularly barium, limits their use in applications where they must be inserted into the human body as particles or fluids.

For high frequency application, the MW dielectric losses of ferrites must be minimized. The dielectric losses due to the damping of the vibration of electrical dipoles, dominate at higher frequencies, causing a high decrease of permittivity in most materials. For that reason, ferrites must have good electrical insulation and moderate permittivity to allow the full penetration of electrical field. Most hexagonal ferrites are better than cubic spinel ferrite with respect to above two properties and therefore are well suited for high frequency applications. In addition to the high operating frequency, current generation electronic devices are becoming smaller with less weight and more efficient day by day. For that, the passive components are used in the form of multilayer chip component and are surface mounted on printed circuit boards.

The compound with greatest technological interest is Y-hexagonal ferrites. Zn_2Y seems to be one of the most suitable for applications in high-frequency device except for its thermal stability [19,20]. The hexaplana ferrites have a preferred direction of magnetization either in the hexagonal basal plane or in a cone and they are excellent soft magnet due to free rotation of magnetisation in the plane/cone. It has been reported that ferrites with planar MCA exhibit good magnetic performance in the GHz range and have higher resonance frequency compared to spinel ferrites.

Chapter 2

LITERATURE REVIEW

Literature Review:

In this section an effort has been made to provide a detailed review of the research work undertaken by various researchers on the synthesis of Co_2-Y($Ba_2Co_2Fe_{12}O_{22}$) and the effect of doping of various divalent cations, in order to synthesize substituted Co_2-Y ,on the magnetic and electric property as well as the effects of various sintering additives on the sintering temperature. Many research works have been carried out to improve the electro-magnetic properties of $Ba_2Co_2Fe_{12}O_{22}$. One of these attempts is by the substitution of various divalent cations like Cu, Zn, Ni, Mn in $Ba_2Co_2Fe_{12}O_{22}$.

The Co_2-Y ferrites have been synthesized through different routes like; conventional solid oxide reaction [21], co-precipitation [22], sol-gel method [23-25], EDTA complexion method [26], etc. The phase formation of these hexaferrites is an extremely complicated process and their formation mechanisms are not yet fully understood. Co_2-Y has been synthesised through conventional solid oxide reaction by calcining oxide raw materials at 1050 ^oC for 3 hours [21].

Magnetic properties of the ferrites depend on many parameters like density, grain size, chemical composition and grain alignment. In general, higher is the density higher will be saturation magnetization (M_s) and lower the grain size higher will be coercive field (H_c). The cation substitution is one of the most important methods for improving magnetic properties of ferrites. *Ms* of the ferrite can be increased by the substitution of non-magnetic Zn^{2+} for Fe^{3+}, where Zn^{2+} prefers tetrahedral positions of the crystal structure. The substitution reduces the negative contribution of tetrahedral-octahedral anti-ferromagnetic coupling. Other 2-valence cations like Cu, Ni, Co, Mg and Mn have also been substituted for Fe^{3+}. The charge compensation for these substitutions is done either by substituting Ba with 3-valence cation or by substituting Fe with 4-valence cation.

The most common substitution in Y-ferrite is $Ba_2Co_{2-x-y}Zn_xCu_yFe_{12}O_{22}$ (x= 0 to 2, y= 0 to 0.8) and the substitution is very important for tailoring anisotropy and microwave properties of Y-ferrite [27]. With the increase in *x*, grain size, M_s *and* H_c decreases. $Ba_2Co_2Fe_{12}O_{22}$ shows excellent antennae characteristics, suitable to cope with a wide MHz range because of higher f_r (over 3 GHz), and it also shows a high curie temperature, Tc ~ 330 ^oC. Substituting with Cu improves the morphology properties of ferrites such as densification; resulting in improved magnetic properties. The magnetic properties of Co_2-Y ferrite will thus be modified

by CuO addition. Zn_2-Y though require a high synthesis temperature, has a large initial permeability in MHz range, which makes it a perfect candidate for substitution purpose. Therefore, $Co_{2-x}Zn_x$-Y hexaferrites seem to be suitable for high frequency applications. The Y-type hexagonal ferrites selected exhibit excellent properties with: high cut-off frequency, high and tunable initial permeability in hyper- frequency range, and low sintering temperature. They show promising future of application in chip inductive components in the hyper-frequency range. It is anticipated that Y-type hexagonal ferrite is a promising high-frequency material for new type of chip electronic component such as multi-layer chip inductors (MLCI) and multi-layer chip beads (MLCB).

Lowering the sintering temperature of the ferrite materials can be realized by either increasing the driving force of sintering or by accelerating the mass transfer during the process. Although there are several methods to lower the sintering temperature, the obtained low-fired samples have different electromagnetic properties. So, it is important to choose the proper low-firing methods or their combinations in practical applications.

The sintering temperature of the ferrites can be reduced to 900 ^oC or less. Two most effective approaches to reduce the sintering temperature are: (1) Use of additives like glass, Bi_2O_3, B_2O_3, SiO_2, for liquid phase sintering, and (2) Partial substitution of metal cations by Cu or addition of CuO. There are only few reports on reduction of sintering temperature of Co_2-Y ferrite by Bi_2O_3 addition, CuO addition, Bi_2O_3-PbO glass, B_2O_3-glass etc.

Shigeo Fuji et. al.[28] reported that after 0.6 wt% CuO addition, Co_2-Y hexagonal ferrite shows a permeability of 2.7 and a loss factor of 0.05 at a frequency of 1GHz. A fabricated ferrite antenna, with a dimension of (3 x 3 x 30) mm with helical printed conductor patterns exhibited excellent average gain of -0.5 dBi at a center frequency of ~600 MHz and showed a wide bandwidth of 160 MHz under a gain level of -5dBi. A dielectric antenna with the same dimension, relative permittivity of 21, line and space pitch 1.25/0.75 and winding of 15 turns was used as a reference.

S. Bierlich and J. Topfer [27] prepared Y-type hexagonal ferrite, $Ba_2Co_{2-x-y}Zn_xCu_yFe_{12}O_{22}$ (x= 0 to 2, y= 0 to 0.8) and obtained single phase Y-hexaferrite after calcining at 1000 ^oC. Samples sintered at 1200 ^oC showed increase in permeability with the substitution of Z for Co and displayed maximum permeability of μ'=35 at 1 MHz for x= 1.6 and y= 0.4, and a resonance

frequency, fr= 500 MHz was observed for zn-rich ferrite with y= 0 and y= 0.4 and the saturation magnetization ‘Ms’ increased.

Addition of Bi_2O_3 shifted the temperature of maximum shrinkage down to T ≤ 950^oC. Moreover an increase in Cu-concentration further lowered the shrinkage temperature ≤ 900^oC enabling co-firing of the ferrites with Ag-metallization for multi-layer technologies. However, low temperature firing reduced μ_r to μ’=10 and the f_r was shifted to 1 GHz.

Objective of the work:

The objective is focussed onto investigating the effects of addition of various sintering additives (B_2O_3, Bi_2O_3, V_2O_5) on the followings:

- formation of phase,
- stability of phase, and
- electrical and magnetic properties of Cu-Znsubstituted Co_2-Y hexagonal ferrite.

Chapter 3

EXPERIMENTAL METHODS

3.1 Synthesis of $Ba_2Co_{0.6}Cu_{0.4}Zn_{1.0}Fe_{12}O_{22}$ ferrite powder

The $Ba_2Co_{0.6}Cu_{0.4}Zn_{1.0}Fe_{12}O_{22}$ ferrite powder was synthesized by solid-state oxide route. Required raw materials $BaCO_3$, Fe_2O_3, CoO, CuO and ZnO were taken by their molar ratio. Then, the precursor mixture was ball-milled for 12h using IPA (propanol) media. Upon drying, the milled powder was then calcinated at 1000°C in air for 4h to get the pure phase ferrite. Fig. 3.1 shows the flow chart for solid-state oxide route of Cu-Zn Co_2Y-ferrite powder synthesis.

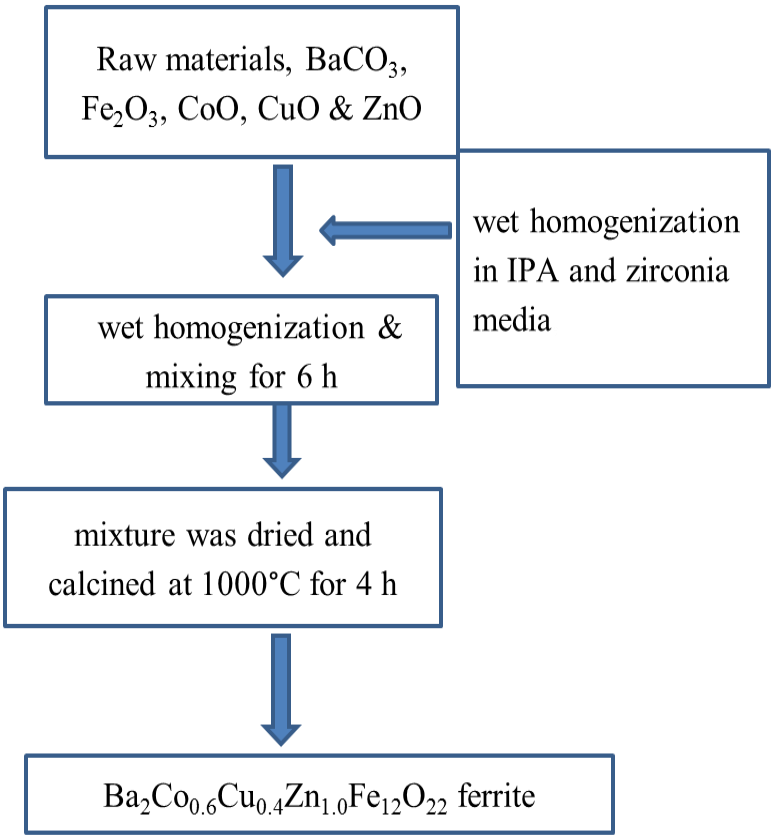

Fig. 3.1 Flow chart for synthesis of $Ba_2Co_{0.6}Cu_{0.4}Zn_{1.0}Fe_{12}O_{22}$ ferrite through solid–state route.

3.2 Ferrite Powder Characterizations

3.2.1 Thermal Characterization

Using the DSC-TG analyser, the thermal decomposition behaviour of raw materials for pure-ferrite powder ($Ba_2Co_2Fe_{12}O_{22}$) was studied.

3.2.2 Phase Analysis

Using Rigaku's X-ray Diffractometer (model: ultima 4, Japan), the phase formation of the powder was studied by X-ray Diffraction pattern. The phases in the samples were identified with the aid of software.

3.3 Samples' Preparation for Sintering

The 1000 ^{o}C calcined powder was wet milled for 12 h and dried to get fine particle size. This milled powder was mixed with different wt% of various sintering additives such as B_2O_3, Bi_2O_3, V_2O_5. Using 5wt% PVA as binder, the powders were uniformly granulated and then pellets with diameter ~13mm & thickness ~2mm with the use of uniaxial press (at pressure of 4 Tonnes/90 seconds) were pressed for sintering studies. The pellets were polled in order to prepare the torroids for measurement and study of permeability. Finally all the samples were sintered at 900^{o}C for 4 hours. The flow chart (Fig.3.2) shows the entire fabrication process of sintered samples and their characterization methods used for analysis of samples.

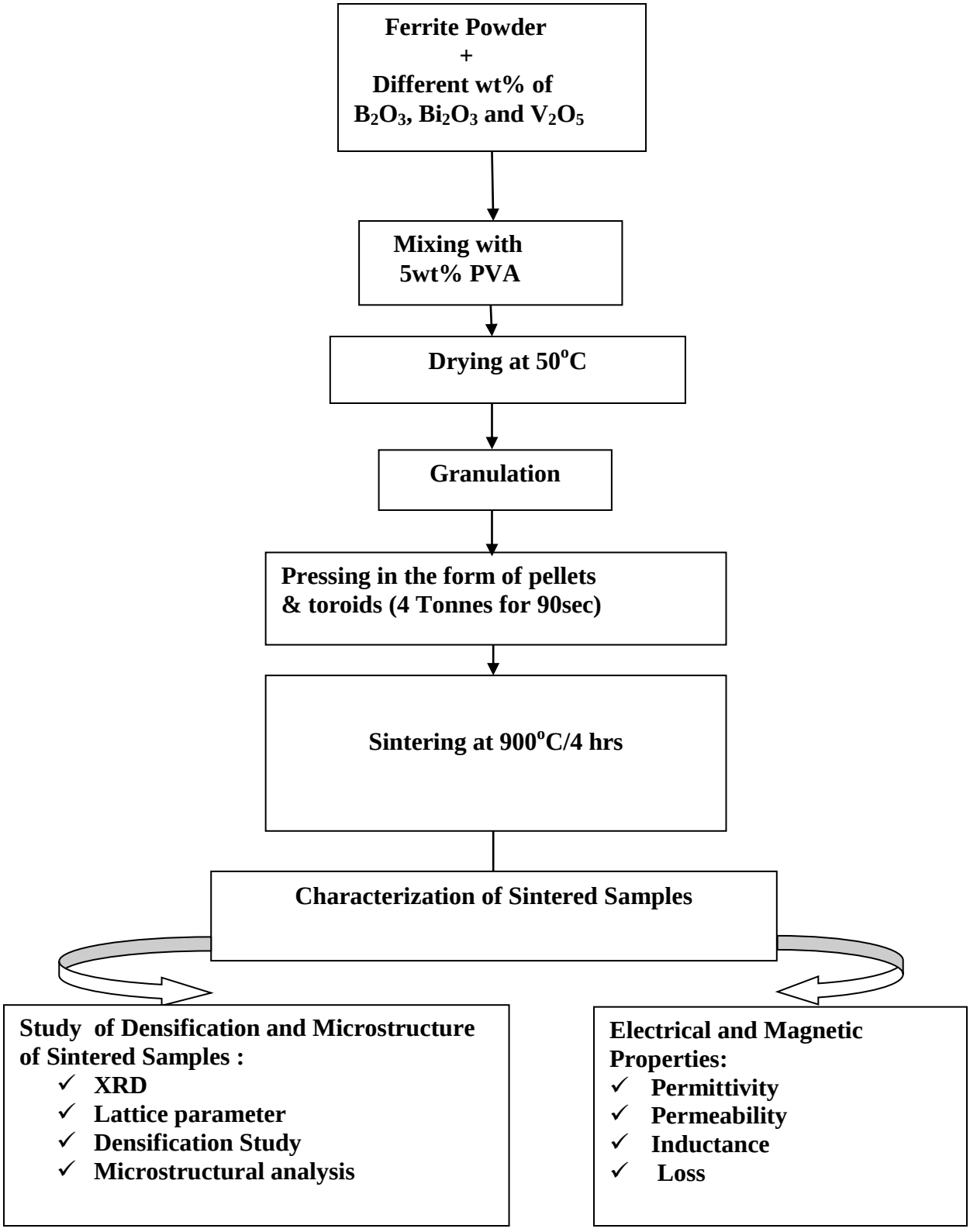

Fig. 3.2. Step-by-step flow chart of: 1) fabrication, and 2) characterization of sintered pellets.

3.4 Characterization of Sintered Samples

After sintering the pellets, phase analysis & microstructural analysis were done. The electrical and magnetic properties of the pellet and toroid specimens were studied and analysed.

3.4.1 Phase Analysis

Using Rigaku's X-ray Diffractometer (model: ultima 4, Japan), the phase formation of the powder was studied by X-ray Diffraction pattern. Then with the help of software, the phases present in the sample were identified.

3.4.2 Densification study

Using NETZSCH dilatometer (model DIL 402 C), rectangular samples' densification kinetics were studied.

The sample holder which is positioned in the furnace's centre holds the rectangular sample in the dilatometer. Inside furnace, the push rod connecting the measuring head, presses against the rectangular sample & records the shrinkage or expansion characteristics. At the rate of 10 ^{o}C/minute, the densification behaviour of different samples were carried-out in air atmosphere for various temperature ranges.

3.4.3 Bulk Density (BD) & Apparent Porosity (AP) measurements

Using Archimedes principle, the BD and AP of sintered pellets were calculated. Dry weight of the sintered samples were noted down. Then, soaked weight of the samples were noted after immersing the same in water and keeping in vaccum under a pressure of 4 mm of mercury for 5 h, ensuring complete filling-up of the pores. The suspended weights of the samples were also measured.

The BD and AP of the samples were calculated using the follow:

$$BD = \frac{D}{W-S} \text{ (g/cc)}$$

$$\text{AP}(\%) = \frac{W-D}{W-S} \text{ x 100 \%}$$

where D, W, S – Dry wt., Soaked wt. & Suspended wt. of the samples respectively.

3.4.4 Microstructural Analysis

Using FESEM (Field Emission Scanning Electron Microscopy), the sintered pellets' microstructures were analysed.

In FESEM, the electron gun emits a beam of e^- in vaccum conditions which falls onto the sample surface after passing through an electromagnetic lenses series. Upon interacting with surface of the sample, a portion of the beam of e^- reflects back as BSE, back scattered electron, and low energy possessing SE, secondary electrons, and some part of the e^- beam gets transmitted.

An image is formed by the SE beam. Then these SE are displayed on a TV screen, which would thus form a bright image if the SE emission is high; due to the surface structures of the samples. Hence, the brightness of the final picture/image so obtained has surface characteristics of the sample being used & the image is generally illuminated.
Metal stub was carbon painted to mount the samples, which were then studied by SEM (FEI).

3.4.5 Dielectric characterization

Using acetone, the sintered pellets were cleaned first. Then the pellets were applied with a silver paste layer (silver plating) on both the sides & cured at 600 ^oC for 1h for dielectric characterization. Dielectric tests of the samples were carried out after curing of the samples.
Using LCR HiTESTER (Model 3532-50) HIOKI, the dielectric behaviours were studied. In frequency ranges of 100Hz to 5MHz, measurements of the test were taken.
The plotted graphs of permittivity vs frequency & tan δ vs frequency were analysed. Here, tan δ is the loss (or dissipation). The relative permittivity, ε is given by:

$$\varepsilon = \frac{C \times d}{\acute{\varepsilon} \times A}$$

where, $\acute{\varepsilon}$ = relative permittivity of air (8.854×10^{-12} F m^{-1}),

C = capacitance of the sample,

d = pellet thickness, and

A = surface area of pellet (top side).

3.4.6 Inductance and Magnetic Loss

Using the LCR HiTESTER (Model 3532-50) HIOKI, the inductance and magnetic loss of the samples were measured. The *tan δ* & the inductance on toroids wound by 6 turns of low capacitive enamelled-copper wire were measured using the instrument. The enamelled-copper wire winding of the core reduces the unwanted capacitance that allows signal leakage between circuital wires.

The ferrite core's inductance depends on variety of factors, like the coil length, number of turn windings, inner & outer diameters of the core and the ferrite's nature. Ratio of total magnetic flux linkage to the current flow through the core is referred to as the inductance of the specimen. Magnetic permeability (μ) dependency of total magnetic flux linkage proves the direct proportionality of inductance to the permeability of the core. Initial permeability of the specimens were enumerated from inductance data using the following formula:

$$\mu' = \frac{L}{2 \times 10^{-7} \times Na^2 \times H_t \times \ln[\frac{D_o}{D_{in}}]}$$

where L = specimen inductance

N_a = number of turns on the toroid

H_t = thickness (width) of toroid

D_o = outer diameter of the toroid

D_{in} = inner diameter of the toroid

Hysteresis loss, eddy current losses and residual losses are the principal losses occurring in the ferrites. The irreversible rotation of magnetization vector is the cause behind the hysteresis losses. The induced current in the ferrite core produces the eddy current loss under the impact of a time varying magnetic flux. Because of the reversible domain wall damping and domain rotations, power loss occurs which causes residual loss.

Chapter 4

RESULTS

AND

DISCUSSIONS

Results and Discussion

4.1 Characterization of Calcined Ferrite Powder

4.1.1 Thermal Characterization

Using the DSC & TG analyser, thermal characterization of the raw material for pure-ferrite powder ($Ba_2Co_2Fe_{12}O_{22}$) was studied. Fig.4.1 shows the DSC and TG curve of the precursor. DSC curve of the powder reveals exothermic peaks at ~261.5 °C, and endothermic peaks at 823 ^{o}C, 896 ^{o}C & 1013 ^{o}C. The TGA curve of the same exhibits 2-step wt. losses, in the range of 50-200 °C and other in the range of 750-1100 °C.

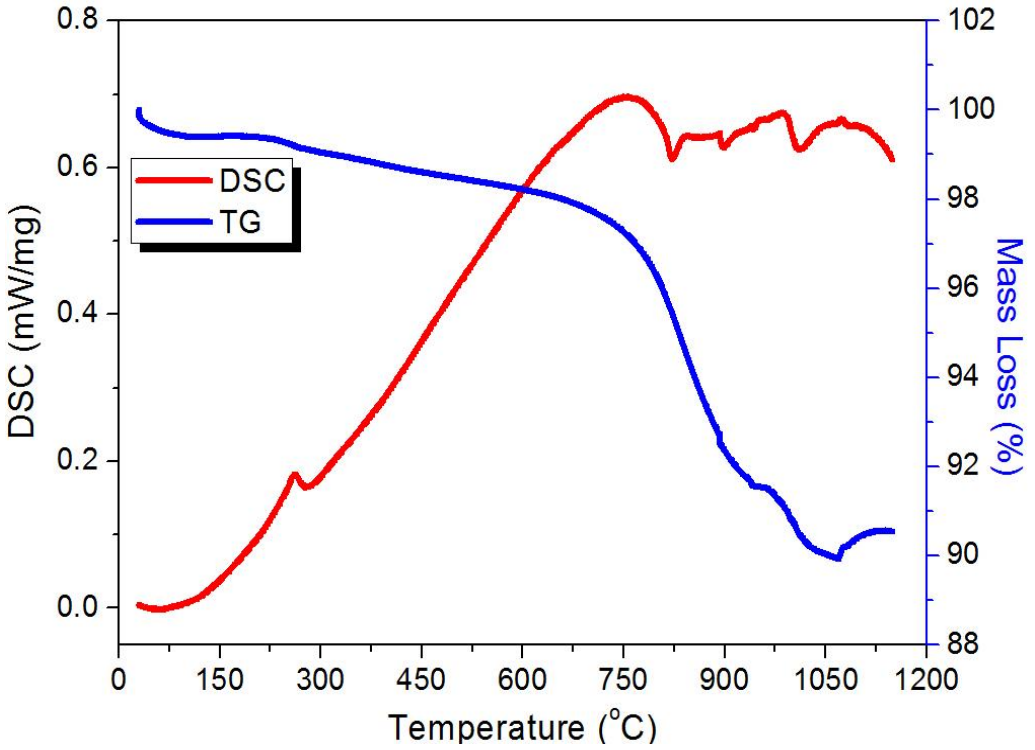

Fig. 4.1. DSC-TG plots of raw material for the $Ba_2Co_2Fe_{12}O_{22}$ ferrite powder with heating rate of 10^{o}C /minute in air atmosphere.

The weight loss in the range of 50-200 °C is due to the removal of moisture from the heated core & that in the 750-1100 °C range is due to the decomposition of $BaCO_3$. The decomposition corresponds to three endothermic peaks as stated above.

The exothermic peak at ~1050 ^{o}C is due to the formation of ferrite phase while that at ~261.5 ^{o}C is may be due to the phase transformation of some raw materials.

4.1.2 Phase analysis of calcined ferrite powder

The figure 4.2 exhibits the X-ray diffraction pattern for calcined powders of $Ba_2Co_2Fe_{12}O_{22}$, calcined at the temperatures of 1050°C, 1100°C, 1150°C and 1200°C respectively.

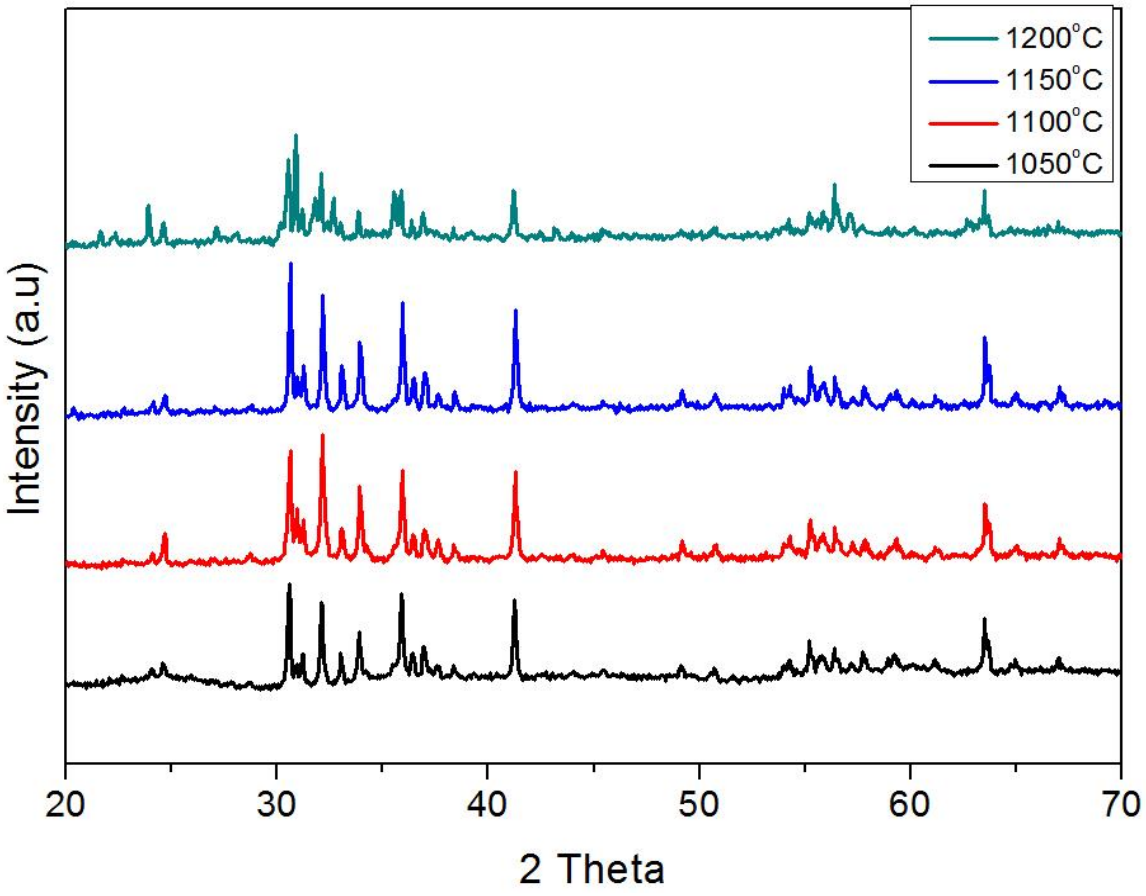

Fig. 4.2 X-ray diffraction patterns of $Ba_2Co_2Fe_{12}O_{22}$ hexaferrite powder calcined at: 1) 1050°C, 2) 1100°C, 3) 1150°C, and 4) 1200°C.

Powders were calcined at different temperatures and phase analysis reveals the formation of Co_2-Y ferrite phase in the powders. Y-phase was obtained at 1000°C. The phase formation reaction may be as follows:

$$6\ Fe_2O_3 + 2\ BaCO_3 + 2\ CoO \longrightarrow Ba_2Co_2Fe_{12}O_{22} + CO_2(g)$$

The ferrite was then substituted with Cu and Zn, to get the desirable composition of $Ba_2Co_{0.6}Cu_{0.4}Zn_{1.0}Fe_{12}O_{22}$. Fig 4.3 shows the XRD pattern for Cu and Zn substituted ferrite specimen . Powders were calcined at various temperatures. The XRD pattern revealed the formation of pure Y-type hexaferrite.

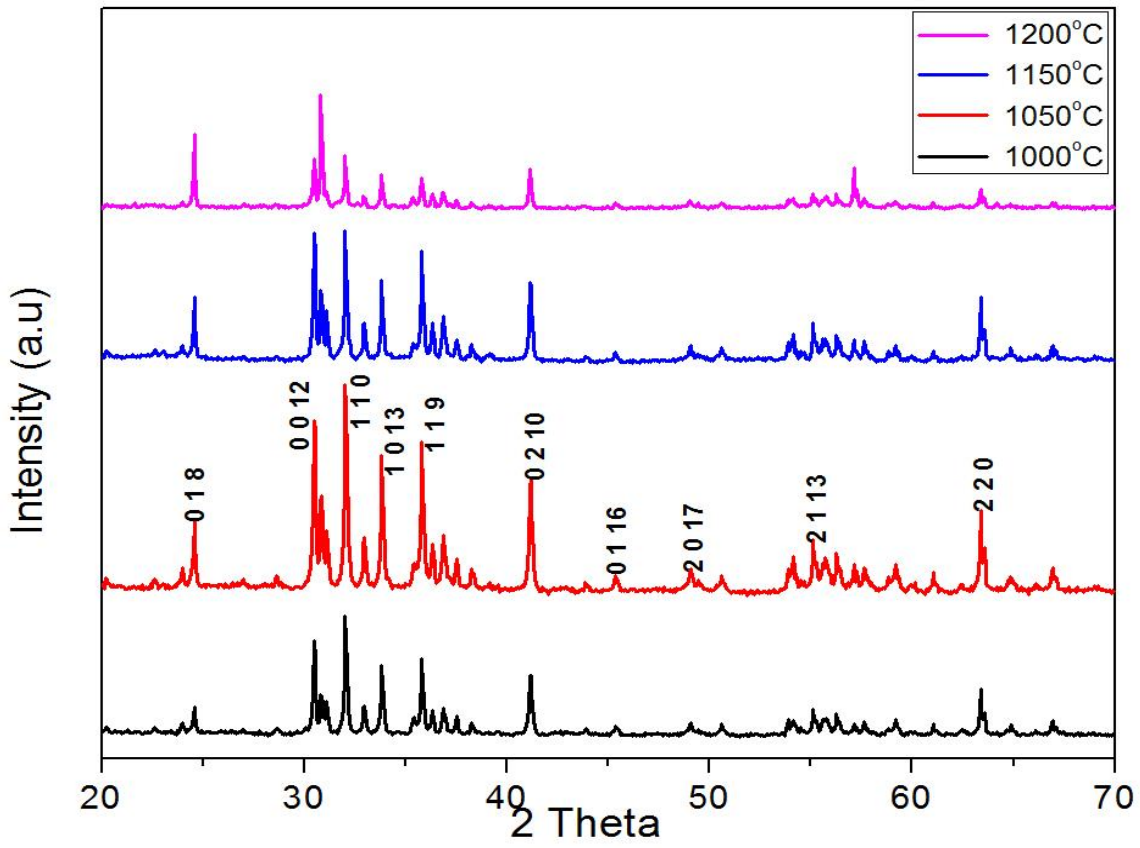

Fig.4.3 X-ray diffraction patterns of Co_2-Y substituted hexagonal ferrite precursor powder calcined at: 1) 1000°C, 2)1050°C, 3) 1150°C, and 4) 1200°C.

The XRD intensity peaks of the powders calcined at various temperatures in the figure shows that with the increase in the calcination temperature, intensity of different peaks change, e.g., the intensity of (0 1 8) peakwas highest in 1200 °C calcined powder. Similarly, other peaks' heights are changing due to the preferential growth of some plane with increase in temperature.

4.2 Characterization of Sintered Pellets

4.2.1 Bulk Density and Apparent Porosity

After sintering of the pellets at 900°C for 4h upon addition of various wt% of the sintering additives used, the apparent porosity and bulk density were measured. Fig. 4.4 and fig. 4.5 exhibit the BD and AP variation with different wt% B_2O_3 & Bi_2O_3 content respectively, for 900°C sintered samples. With addition of various wt% of the both the additives, BD normally increases

and AP decreases as shown. The bulk densities of 5 wt% B_2O_3 and (2.5+2.5) wt% (B_2O_3 + Bi_2O_3) are almost similar as shown in the plot, (2.5+2.5) being slightly higher.

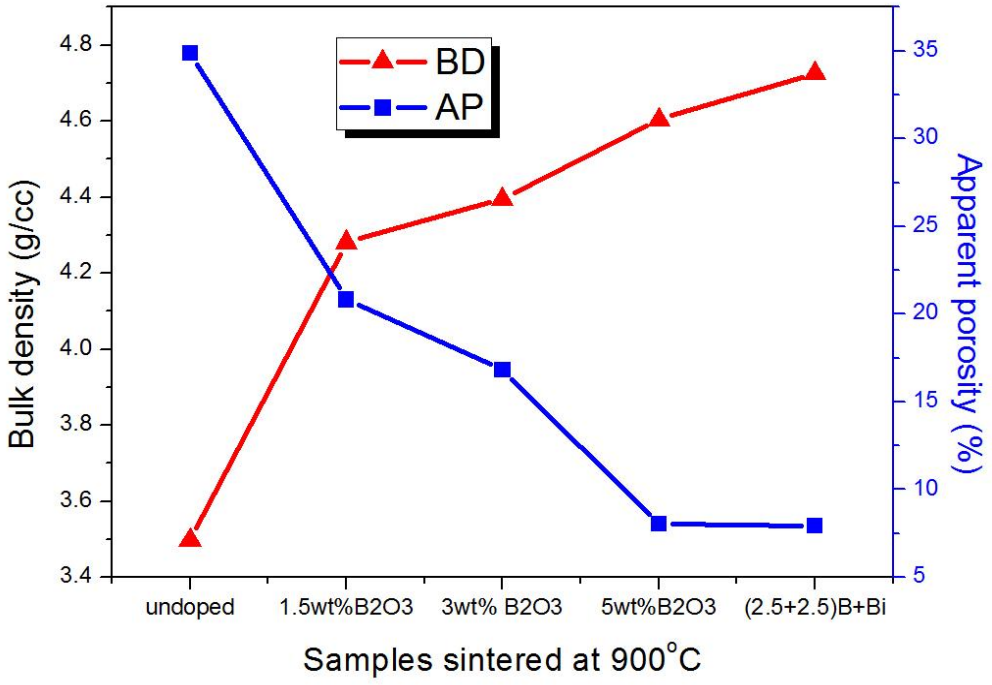

Fig. 4.4. BD and AP variation with different wt% B_2O_3 content for 900°C sintered samples.

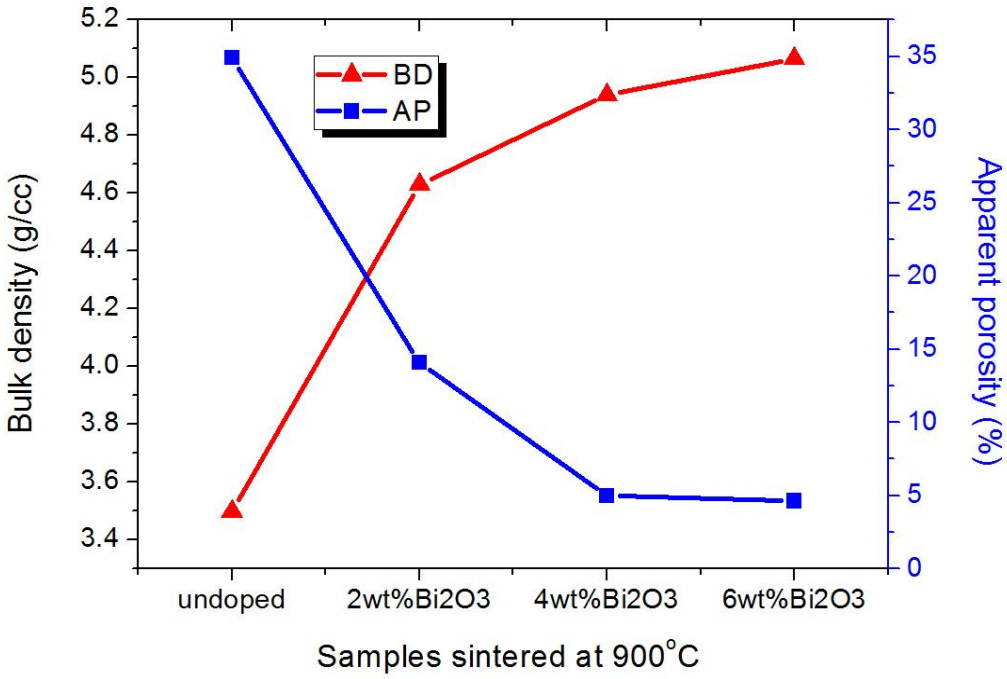

Fig. 4.5. BD and AP variation with different wt% Bi_2O_3 content for 900°C sintered samples.

The experimental results exhibit that apparent porosity decreases while bulk density increases with increase in B_2O_3 and Bi_2O_3 contents because of the lower melting point of B_2O_3 and Bi_2O_3, which melt prior to sintering and enhances liquid phase sintering and thus better densification occur. Liquid phase sintering is a process where a secondary phase (liquid at elevated/fabrication temperatures) is used in the body to enhance densification. Typically the liquid phase volume is of few percent. Liquid phase sintering enhances densification (as compared to solid state sintering) by better rearrangement of particulate solids. Because of the liquid bridge, friction between particles is reduced, which leads to better rearrangement. Assuming that the liquid phase wets the solid particles, the solid-vapor interface is eliminated and pores with the liquid-vapor interface. Therefore, the reduction of the liquid-vapor interface (or the elimination of porosity) provides the driving force for sintering.

The BD of Bi_2O_3 added pellets are higher than that of B_2O_3 added pellets, which concludes that Bi_2O_3's effect in aiding the sintering process is higher. However the V_2O_5 added pellets showed very little variation of porosity and density for the different wt% studied, as shown in fig. 4.6.

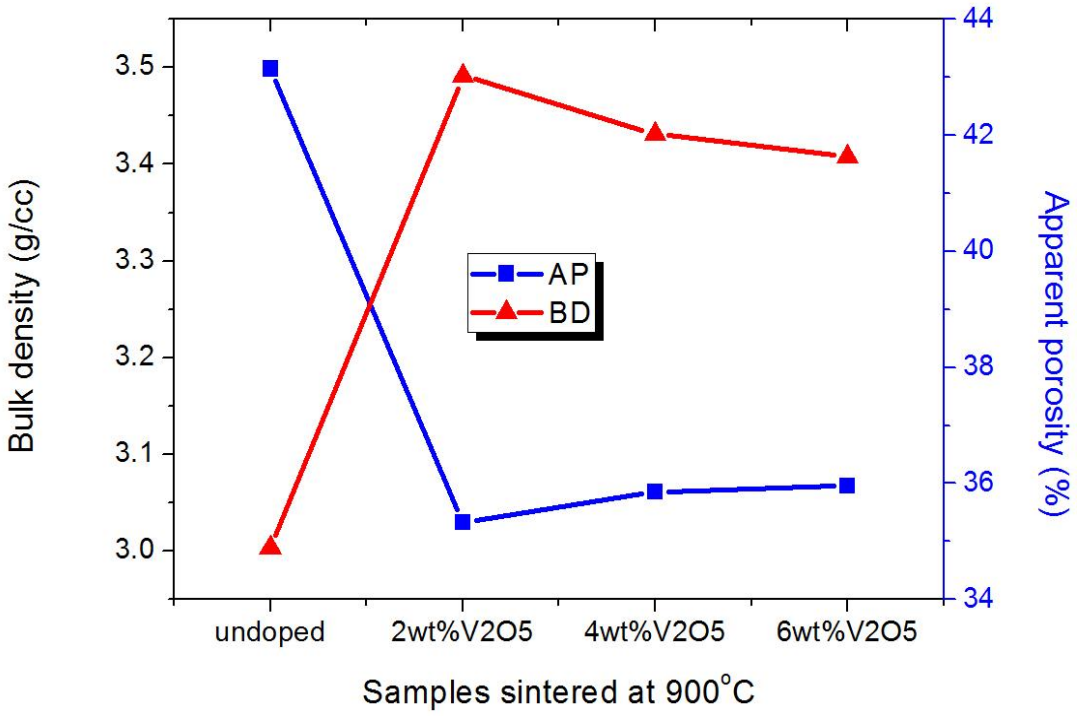

Fig. 4.6. BD and AP variation with different wt% V_2O_5 content for 900°C sintered samples

Since the V_2O_5 added pellets (different wt%) sintered at 900^oC showed negligible differences, the pellets from the three different wt% of V_2O_5 were sintered at further higher temperatures, 1000 ^oC and 1100 ^oC. The corresponding AP and BD of the pellets were measured and studied.

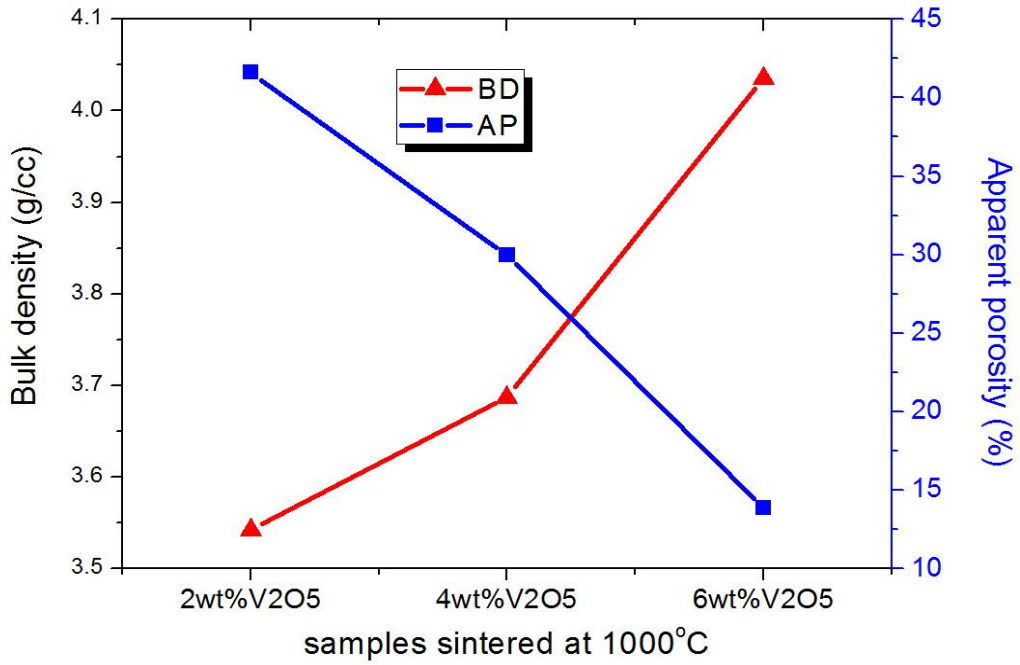

Fig. 4.7. BD and AP variation with different wt% V_2O_5content for 1000^oC sintered samples.

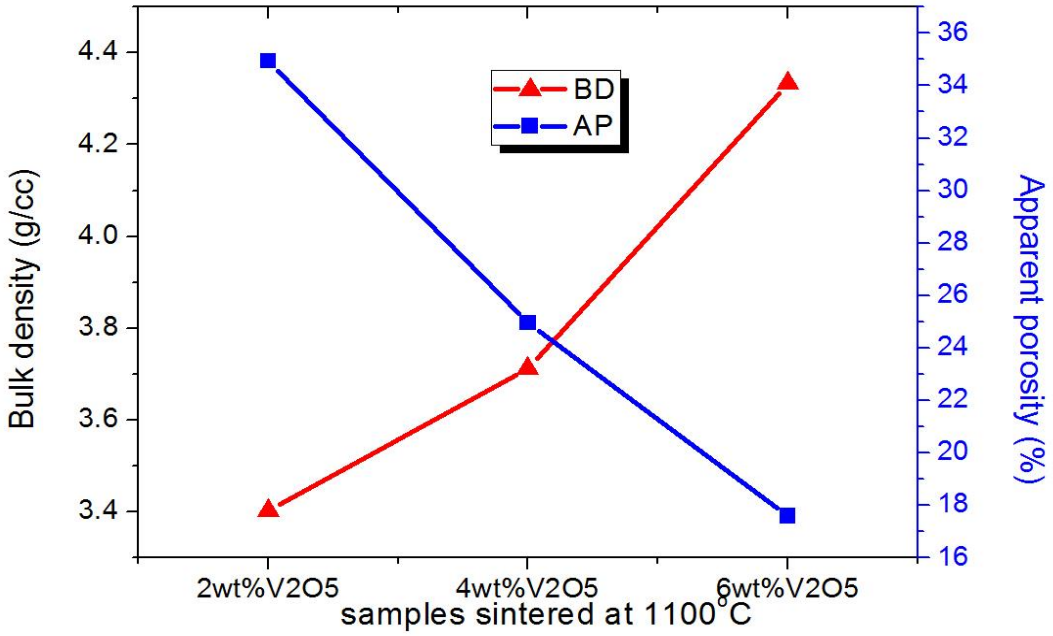

Fig. 4.8. BD and AP variation with different wt% V_2O_5content for 1100^oC sintered samples.

Fig. 4.7 and fig. 4.8 exhibit the BD and AP variation of samples with different wt% V_2O_5, sintered at 1000°C and 1100°C respectively. The bulk density increased with increase in wt% of V_2O_5 while the apparent porosity decreased, for both 1000°C and 1100°C. The bulk density of the pellets sintered at 1100°C were higher that those of the respective pellets sintered at 1000°C, while that of apparent porosity decreased than those at 1000°C. The 6 wt% V_2O_5 added pellets are having slightly higher BD than those of the 4wt% V_2O_5 added pellets, which is higher than those of 2wt% V_2O_5 added pellets. The AP of 6wt% V_2O_5 added pellets are lower than those of 4wt% V_2O_5 added pellets, which is lower than those of the 2wt% V_2O_5 added pellets.

All these data show that V_2O_5 sintering additive is not so effective in assisting the liquid phase sintering at 900 °C, as it has the lowest BD which is in the range of 3.4 to 3.5, whereas the BD for Bi_2O_3 containing specimens were in the range of 4.6 to 5.0 & the BD for B_2O_3 containing specimens were in the range of 4.2 to 4.6. These indicate that Bi_2O_3 is the most efficient sintering additive for this substituted Co_2Y hexaferrite and B_2O_3 is an intermediate one between Bi_2O_3 and V_2O_5.

4.2.2 Linear Shrinkage

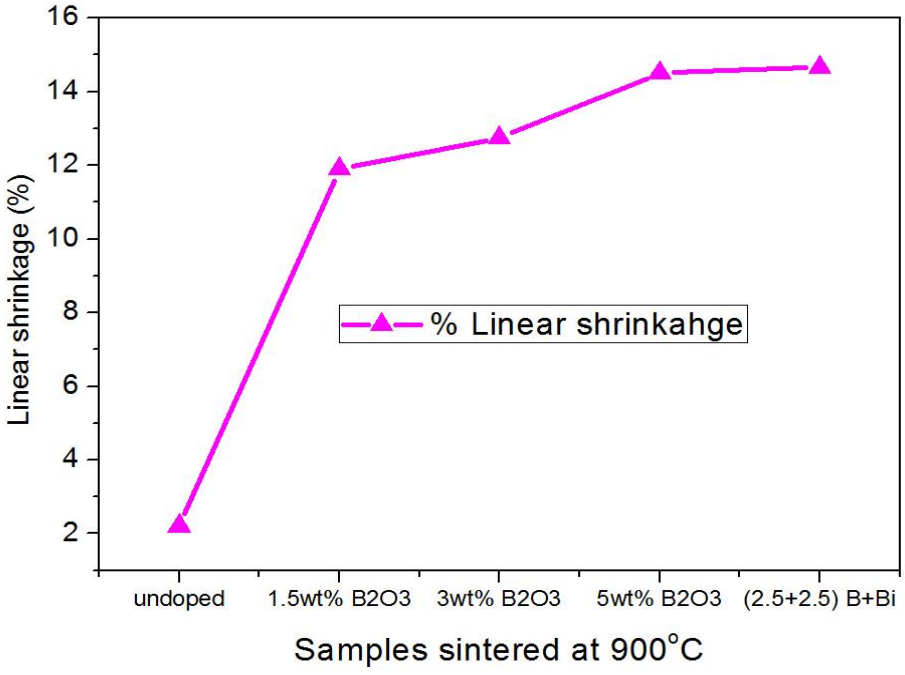

Fig.4.9. Percentage Linear shrinkage curve with variation of B_2O_3 wt% in $Ba_2Co_{0.6}Cu_{0.4}Zn_{1.0}Fe_{12}O_{22}$ ferrite .

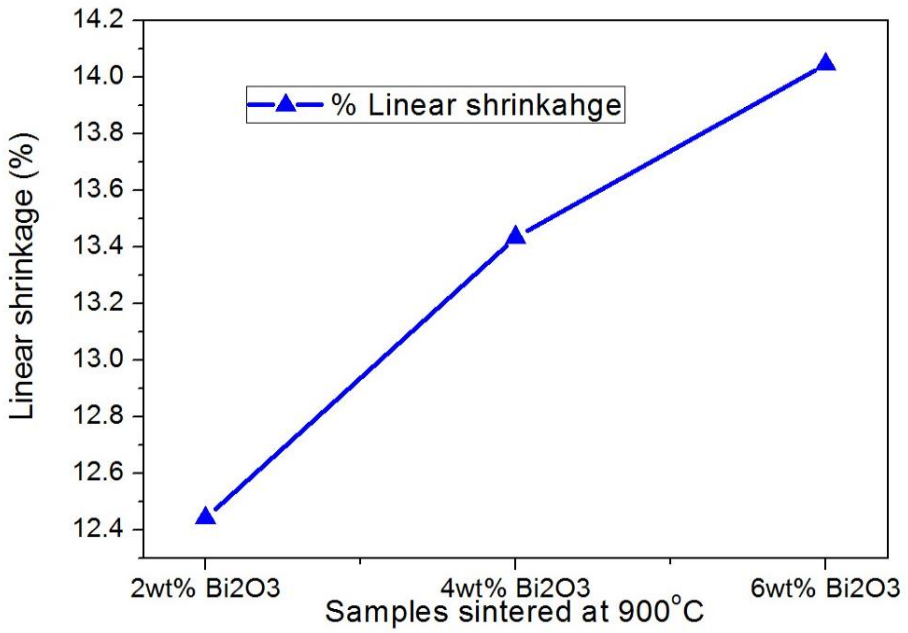

Fig.4.10. Percentage Linear shrinkage curve with variation of Bi_2O_3 wt% in $Ba_2Co_{0.6}Cu_{0.4}Zn_{1.0}Fe_{12}O_{22}$ ferrite.

The linear shrinkage of the pellets was measured by measuring the initial green-pellet diameter and final sintered-pellet diameter. Fig 4.9 & 4.10 shows the Percentage Linear shrinkage curve for variation of B_2O_3 and Bi_2O_3 added ferrite. The shrinkage of both additive added pellets increased from lower wt% to higher wt% of the corresponding sintering aids. The shrinkage in 5wt% B_2O_3 and (2.5+2.5) wt% were almost similar, the mixed type being slightly higher. The shrinkage % in case of Bi_2O_3 added pellets were more than those of the B_2O_3 added pellets.

Fig.4.11 exhibits the Percentage Linear shrinkage curve for ferrite with variation of V_2O_5 wt%. The V_2O_5 added pellets sintered at 900°C revealed very little shrinkage (nearly 0%). However, shrinkage of the pellets sintered at 1000°C and 1100°C increased as the wt% increased. At 1100°C, shrinkage of the pellets sintered was noticeable as the wt% increased from 2 to 6wt%.

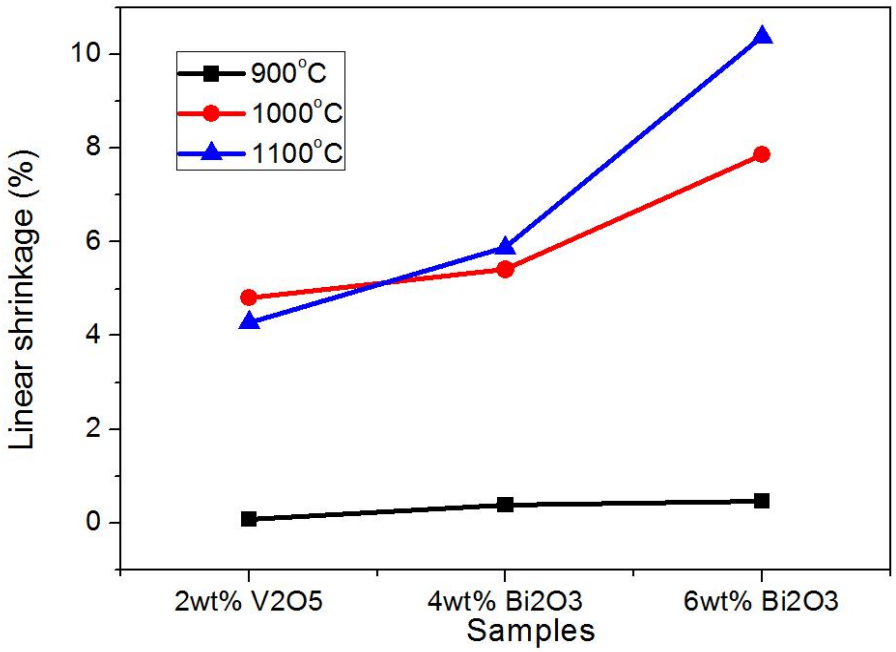

Fig.4.11. Percentage Linear shrinkage curve with variation of V_2O_5 wt% in $Ba_2Co_{0.6}Cu_{0.4}Zn_{1.0}Fe_{12}O_{22}$ ferrite .

In case of V_2O_5, there is a wide gap in linear shrinkage in-between 900 to 1000 °C. So, 900 °C is not at all suitable for V_2O_5, i.e., the sufficient amount of liquid phase is not forming at 900 °C. So, it may be concluded that if V_2O_5 is to be used as a sintering additive, the sintering temperature of ≥1000 °C is to be applied. After that, the shrinkage of the specimens will be normal.

4.2.3 Dilatometry Analysis

Fig.4.12 shows the dilatometry curves, i.e., the densification behaviour (or shrinkage behaviour) of rectangular samples with application of temperature. The curves are exhibiting similar fashion for all the sample compositions. Basically, the sintering additives are added in various ferrite compositions during sintering to form low eutectic liquid compositions.

The figure exhibits that in the case of undoped ferrite composition, the sintering starts at ~950°C. With the addition of sintering additives, the shrinkage temperature lowers down, e.g., the shrinkage of 5wt% B_2O_3 specimen starts at ~850 °C which is 100°C lower than the undoped specimen. This is due to the formation of liquid phase by addition of B_2O_3 and liquid phase assisted sintering of ferrite.

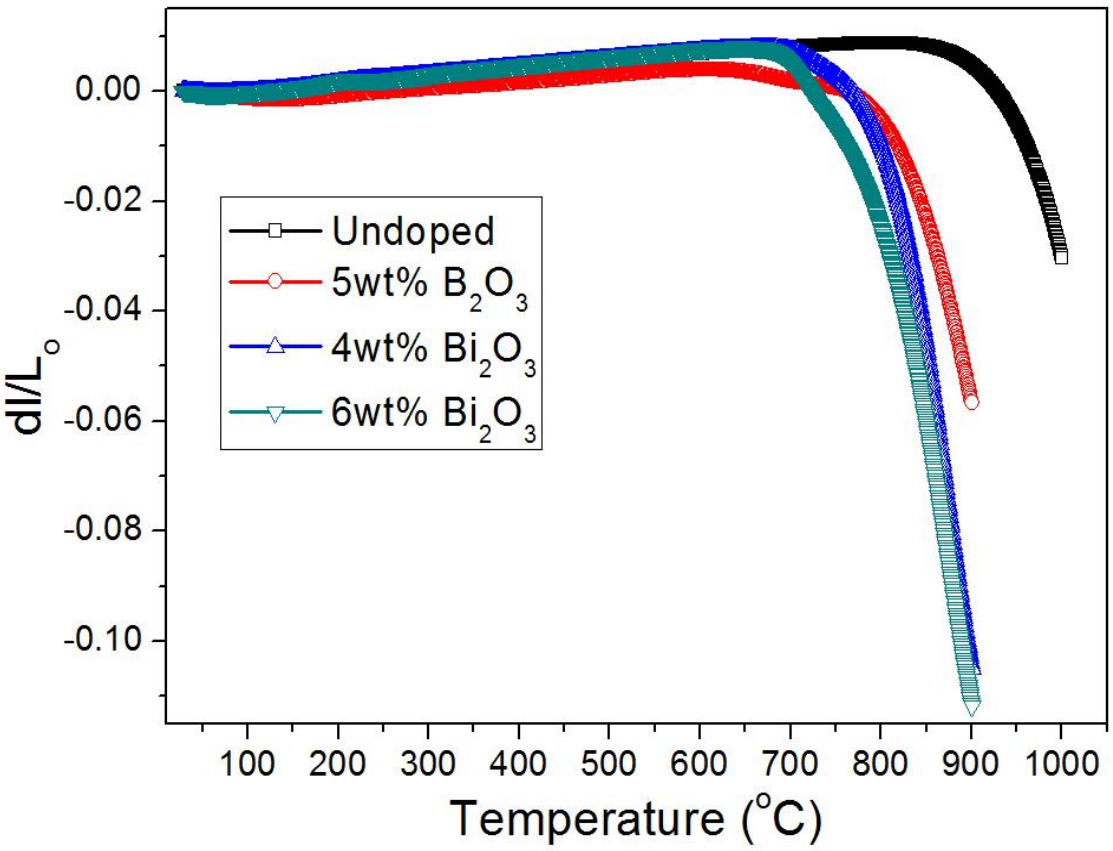

Fig.4.12 Dilatometry curves for different powder compositions synthesized upon addition of the sintering additives.

However, Bi_2O_3 seems to be a better sintering additive than B_2O_3 as the shrinkage of 4wt% Bi_2O_3 starts at ~750 ^oC and that sintering temperature again decreases with the increase in Bi_2O_3 content as the figure shows that 6wt% Bi_2O_3 containing specimen has the lowest sintering temperature. So, it may be concluded that 4wt% Bi_2O_3 will be an optimum sintering additive for the ferrite.

4.2.4 Phase Evolution in Sintered Pellets

Fig. 4.13 shows the X-ray diffraction pattern of 900^oC sintered $Ba_2Co_{0.6}Cu_{0.4}Zn_{1.0}Fe_{12}O_{22}$ ferrite which were doped with different amount of B_2O_3. All the XRD patterns are matched with the pure Y- type phase with the JCPDS no-44-0206. There is no secondary phase formation or decomposition of ferrite phase. So that B_2O_3 can be a good sintering additive to lower down the sintering temperature to 900^oC without harming the pure phase of ferrite.

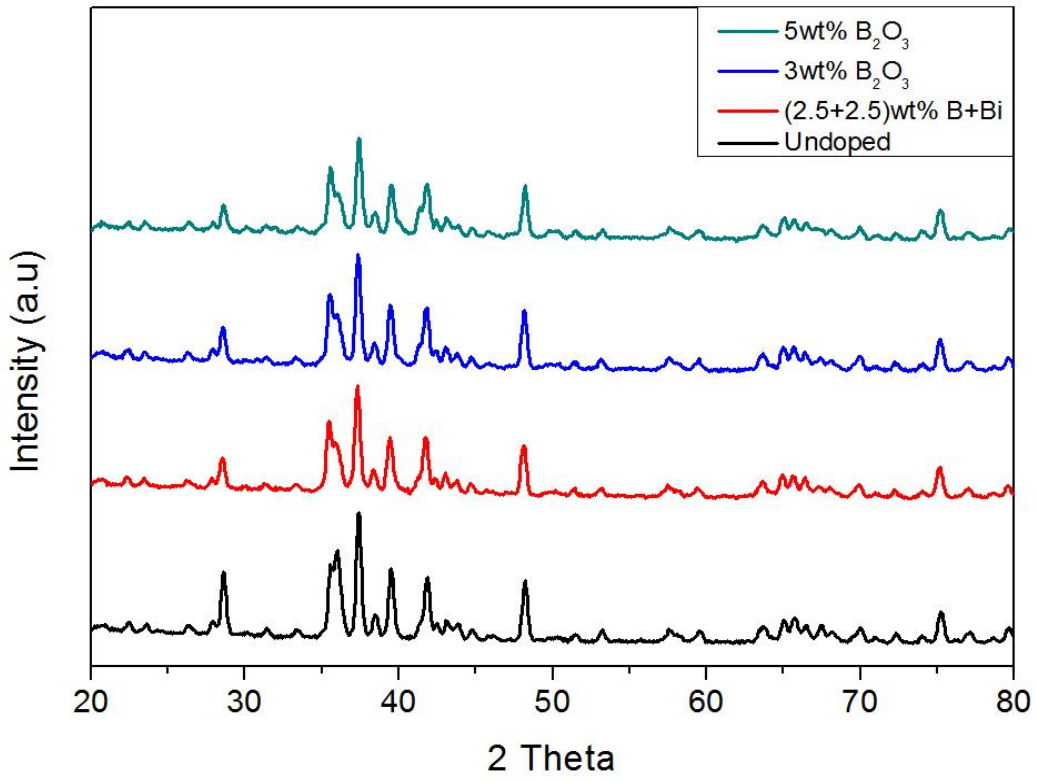

Fig.4.13. X-ray diffraction pattern of 900°C sintered Co_2-Y substituted hexaferrite precursor with different wt% of B_2O_3: (a) Undoped, (b)(2.5+2.5)wt% B+Bi , (c) 3wt%, and (d) 5wt%.

Fig. 4.14 shows the X-ray diffraction pattern of 900°C sintered $Ba_2Co_{0.6}Cu_{0.4}Zn_{1.0}Fe_{12}O_{22}$ ferrite which were doped with different amount of Bi_2O_3. The all XRD patterns are matched with the pure Y- type phase with the JCPDS no-44-0206. There is no secondary phase formation or decomposition of ferrite phase. So that Bi_2O_3 also be another good sintering additive to lower the sintering temperature to 900°C without harming the pure phase of ferrite.

Fig. 4.15 shows the X-ray diffraction patterns of 1100°C sintered $Ba_2Co_{0.6}Cu_{0.4}Zn_{1.0}Fe_{12}O_{22}$ ferrite along with 6wt% of V_2O_5. The XRD pattern of doped ferrite shows secondary phases formation or decomposition of ferrite phase. So that V_2O_5 not suitable sintering additive to reduce the sintering temperature to 900°C due to harming the pure phase of ferrite.

Phase analysis was done to access the stability of ferrite in the presence of liquid phase created by the addition of sintering additives. It has been found that the phase of all the samples with various wt% of the sintering aids sintered at 900 °C are stable.

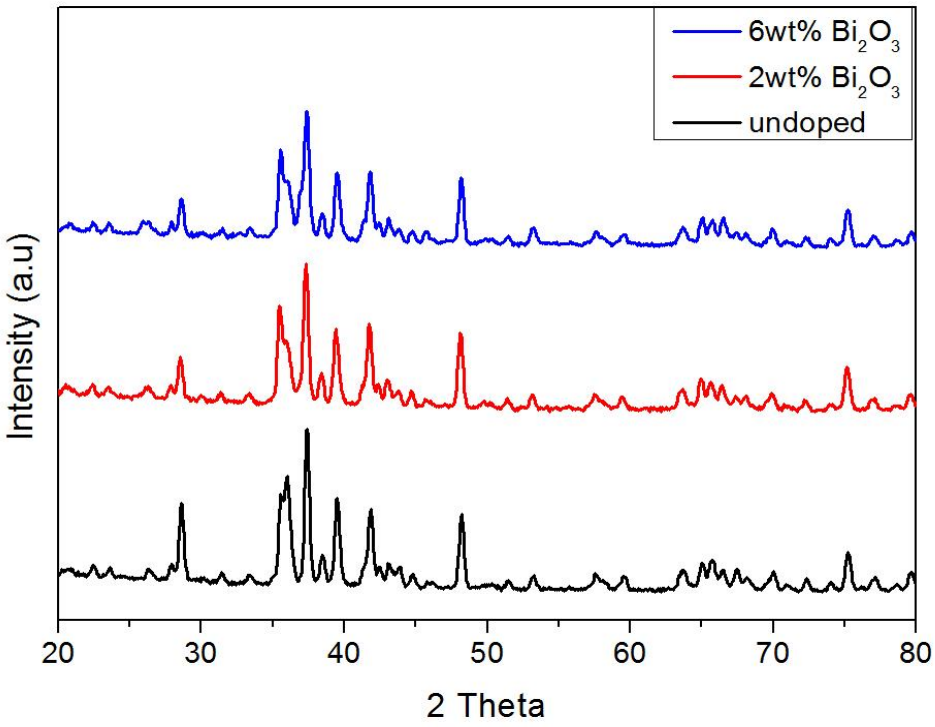

Fig.4.14. X-ray diffraction pattern of 900°C sintered Co_2-Y substituted hexaferrite precursor with different wt% of Bi_2O_3: (a) Undoped, (b)2wt%, (c) 6wt%.

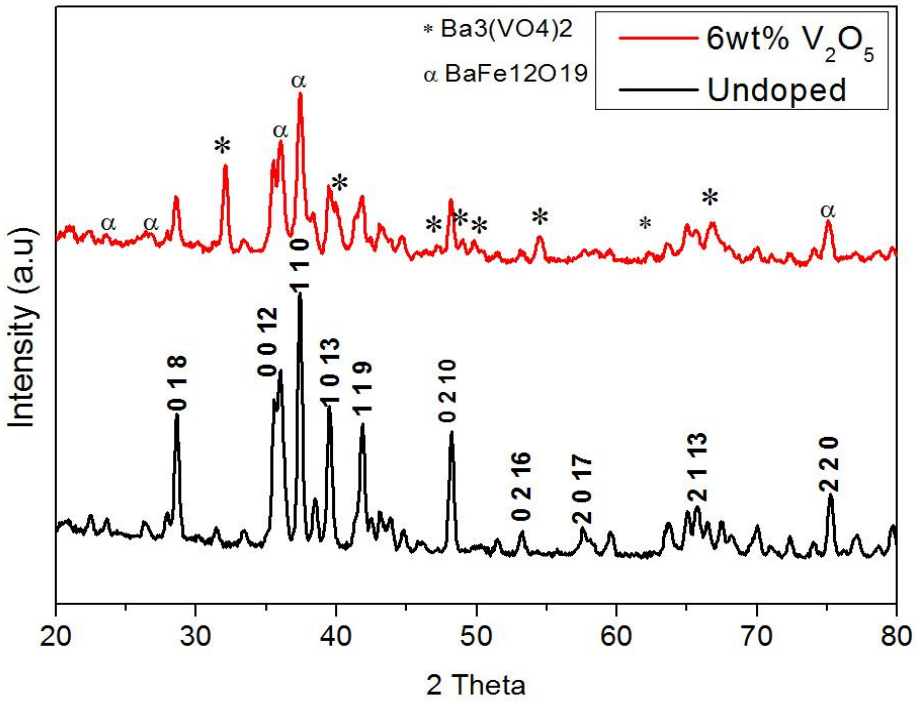

Fig.4.15. X-ray diffraction pattern of 1100°C sintered Co_2-Y substituted hexaferrite (a) Undoped, (b) 6wt% of V_2O_5 added.

4.2.5 Microstructural Analysis

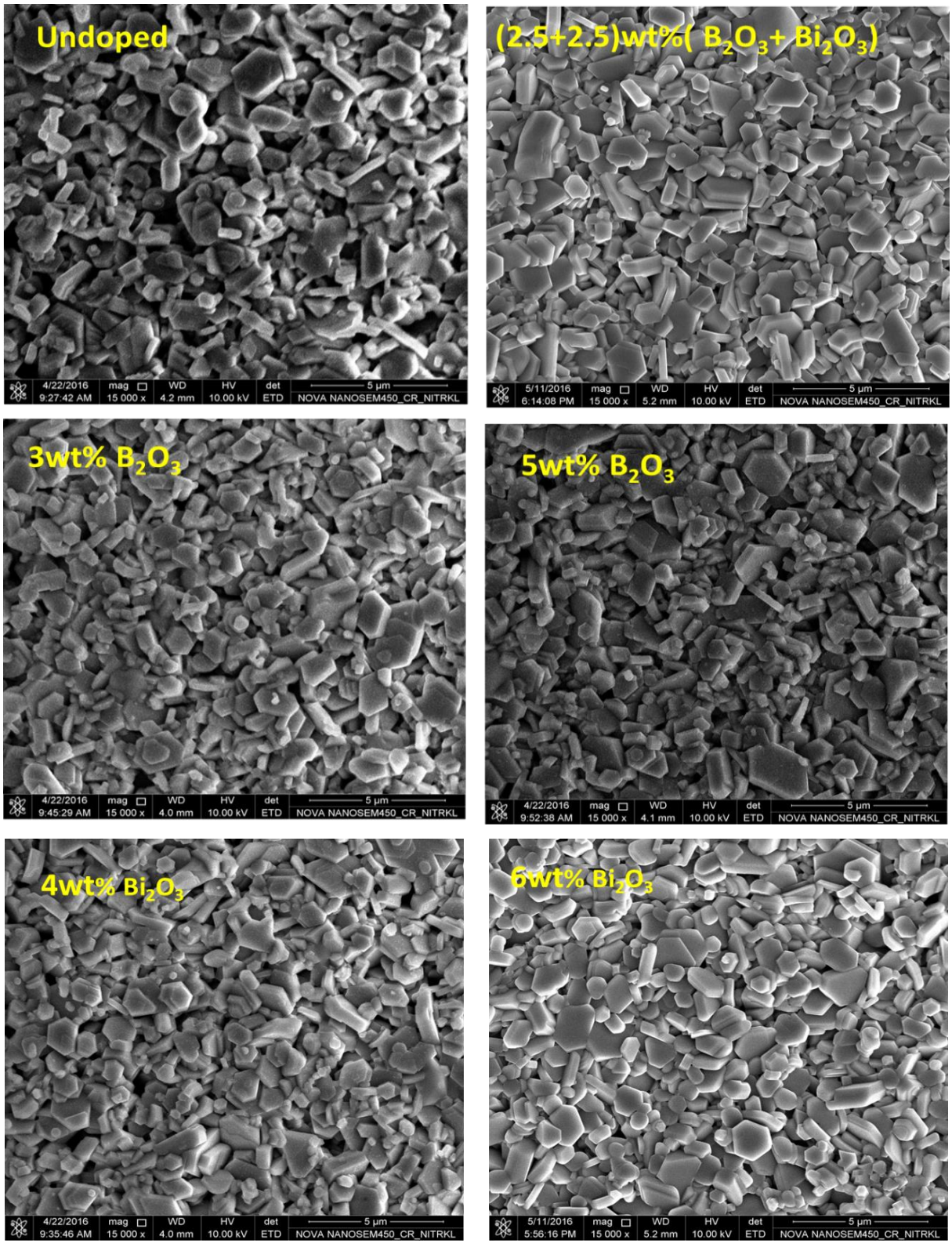

Fig. 4.16. SEM micrograph of 900^{o}C sintered ferrite with different wt% sintering additive.

Fig 4.16 exhibits SEM micrograph of 900°C sintered ferrite with different wt% B_2O_3 and Bi_2O_3. The microstructues shows the formation of hexagonal plate like grains, which is the typical characteristic of hexagonal ferrite, with average grain size of around 1-2µm. The grain size of the ferrite was highest in case of 6wt% Bi_2O_3 Fig 4.16(f), also the porosity was lowest. The Bi_2O_3 added sample shows more uniform and dense microstructure than B_2O_3 added samples, this may be due to lower wetting behavoir of grain boundry in case of B_2O_3 during sintering.

4.2.6 Electrical Properties analysis

4.2.6.1 Permittivity

Fig. 4.17 exhibits the typical phenomenon of decrease in permittivity of the specimen from lower frequency region to higher frequency region. The plot reveals that permittivity increases as the content of B_2O_3 and Bi_2O_3 increases in the specimens, and it is almost constant. This may be due to higher densification and lower porosity of ferrite. This behaviour is mostly related to the density of the specimens; as density of the specimens increases, the permittivity also increases.

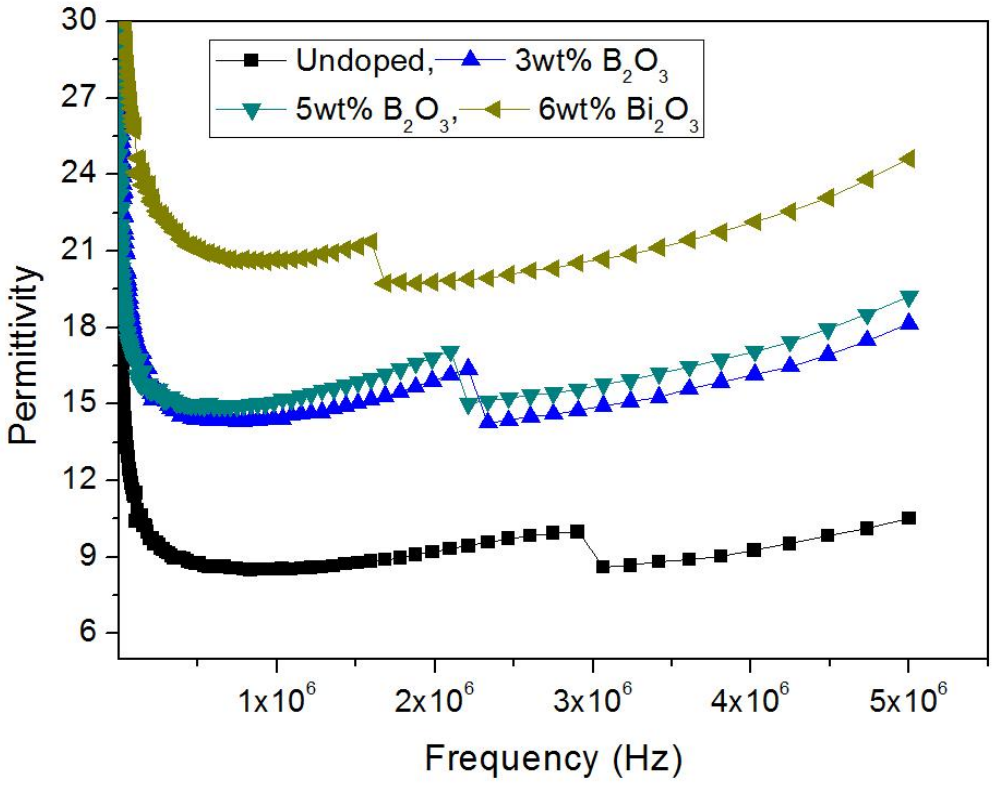

Fig. 4.17 Frequency dependency of permittivity in ferrites with different sintering additive content.

4.2.6.2 Dielectric Loss

Fig. 4.18 shows the variation of dielectric loss (tan δ) with frequency. The figure exhibits that the dielectric loss is almost constant with increase in frequency. The addition of B_2O_3 and Bi_2O_3 results in lower dielectric loss because of increase in density of the sample in higher frequency region.

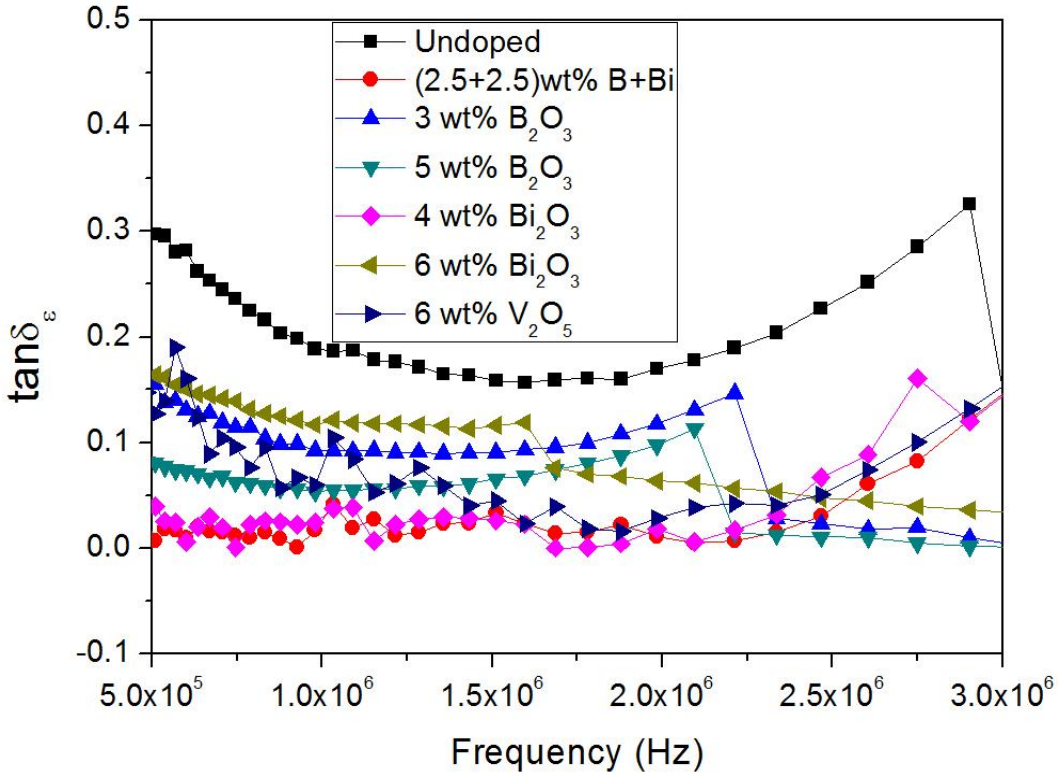

Fig.4.18 Dielectric loss of pellets with frequency

4.2.6.3 Impedance analysis

Fig. 4.19 shows that Impedance decreases with increase in B_2O_3 and Bi_2O_3 added samples, indicates that 6 wt% Bi_2O_3 specimen has lowest impedance. Hexaferrites start decomposing with the addition of V_2O_5 in the specimens. The decomposed non-magnetic products persist in the grain boundary. The increase in impedance with increase in V_2O_5 content may be accredited to the presence of non-magnetic grain boundary phases.

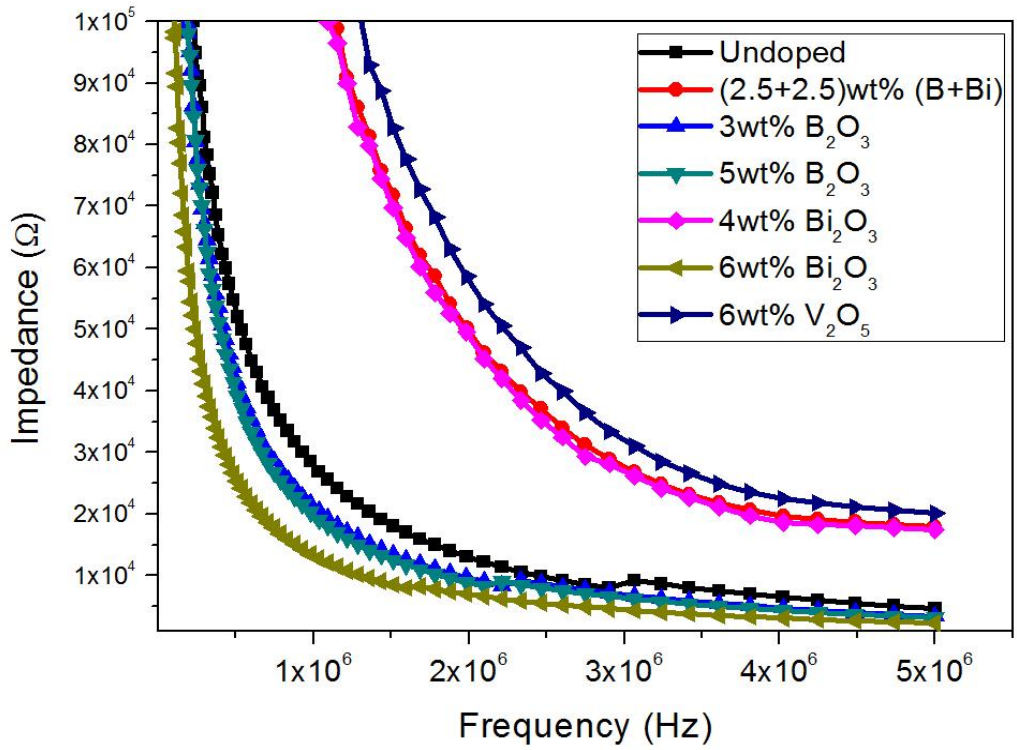

Fig. 4.19. Frequency dependency of impedance in ferrite pellets with different sintering added ferrite

4.2.7 Magnetic Properties

4.2.7.1 Initial Permeability

Fig. 4.20 exhibits the frequency dependency of initial permeability. As frequency is increased, the initial permeability of the specimens decreases due to the restriction of switching of magnetic domains by domain walls leading to a significant decreased response. As the sintering additives content increased, decrease in permeability is remarked. The lower initial permeability at higher frequencies in 5wt% B_2O_3 ferrites compare to other composition.

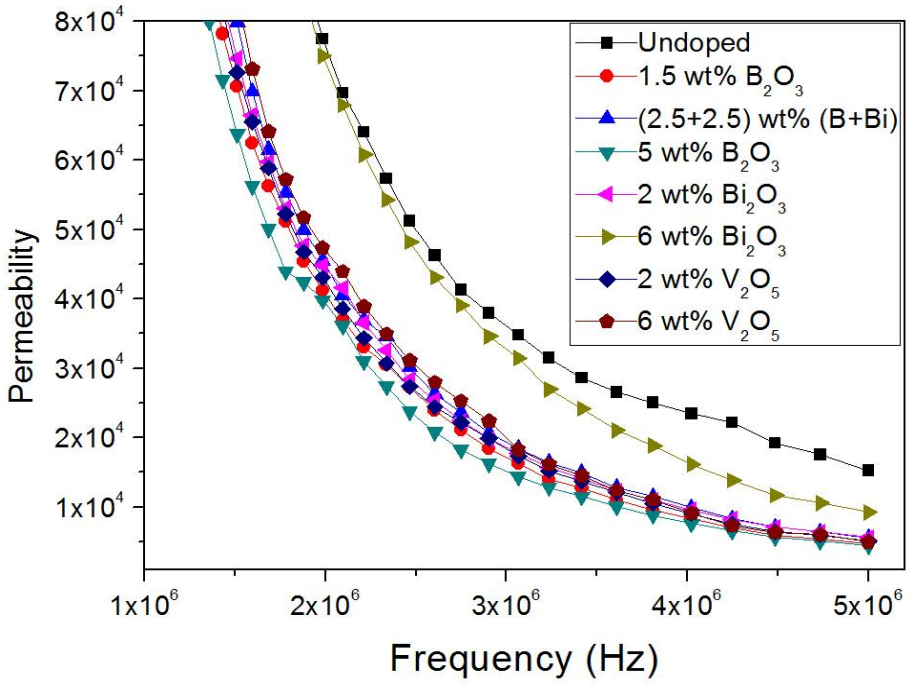

Fig. 4.20. Frequency dependency of initial permeability for toroids with different sintering additives

4.2.7.2 Relative Loss Factor

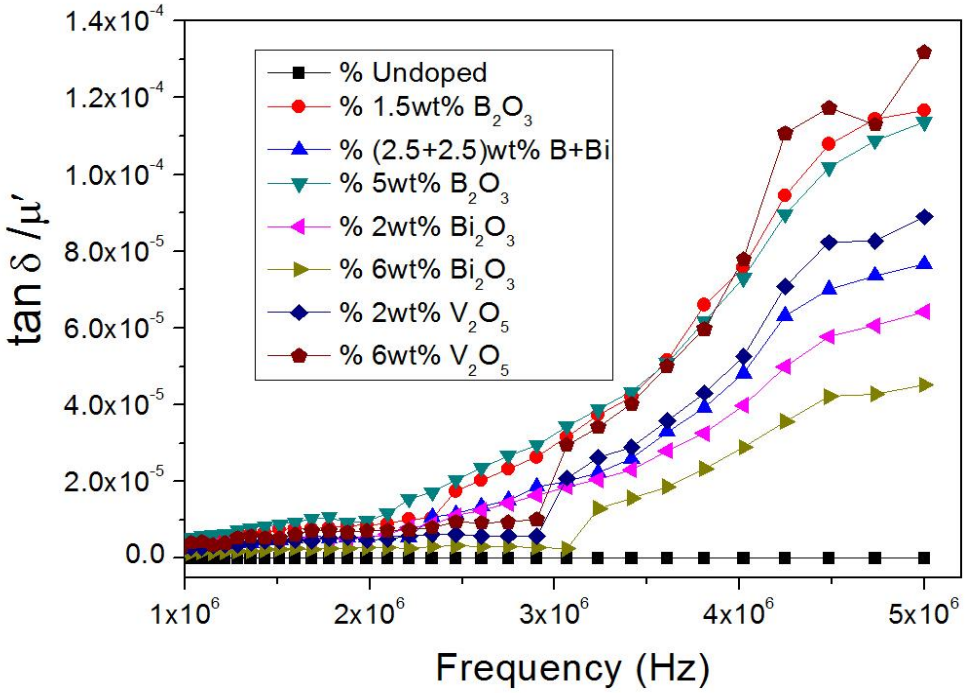

Fig.4.21 Frequency dependency of relative loss factor for torroids of different wt% sintereing additive added ferrite.

Relative Loss Factor (RLF) is referred to the ratio of magnetic loss (tan δ) to initial permeability (μ'), which is a principal parameter for the inductors to be used at higher frequency and a low RLF is desirable. Fig.4.21 exhibits the frequency dependency of relative loss factor of the specimens. With increase in frequency, RLF increases, which also increases with the wt% of V_2O_5. The ferrite without sintering additive has lowest RLF. The 6wt%Bi_2O_3 added sample showing similar behaviour of undoped ferrite, which is may be due to highest densification exhibited by the same.

As the wt% of the sintering additives in the composition increased, there is an increase in inclusion of non-magnetic phases in the specimens. As the volume of non-magnetic phases increase, the initial permeability decrease, which is the reason behind the increase in RLF.

Chapter 5

CONCLUSION

Conclusion

The Cu–Zn co-substituted Co_2-Y ferrite ($Ba_2Co_{0.6}Cu_{0.4}Zn_{1.0}Fe_{12}O_{22}$) ferrite was synthesized by solid oxide route. The XRD result confirms the formation of pure phase at 1000^oC. The effects of B_2O_3, Bi_2O_3 and V_2O_5 sintering additives on sintering temperature, phase stability, microstructure and dielectric & magnetic characteristics of the ferrites were studied and analysed. Ferrite with Bi_2O_3 additives showed better shrinkage and densification at 900°C, than B_2O_3 and V_2O_5; V_2O_5 additive had very little effect (less than 5%) on the sintering behavior when sintered at 900^oC. However, the ferrite phase decomposed with an addition of 6 wt% V_2O_5, when fired at 1100^oC . The higher sintering rate and lower sintering temperature was found in B_2O_3 and Bi_2O_3 added ferrites. There was very little densification in the case of undoped and V_2O_5 doped specimen when sintered at 900°C, while denser microstructure and increased grain growth were observed in the case of the higher B_2O_3 and Bi_2O_3 wt %-content samples.

Chapter 6

REFERENCES

REFERENCES:

[1] Smit J, Wijn HPJ. Ferrites, Philips Technical Library, Eindhoven; 1959.

[2] Robert C. Pullar, Progress in Materials Science 57 (2012) 1191–1334.

[3] Braun PB. Philos Res Rep 1957;12:491.

[4] Sugimoto M. In: Wohfarth EP, editor. Ferromagnetic materials, vol. 3. Amsterdam: North-Holland Physics Publishing; 1980. p. 392–440.

[5] Slowak R, Voight C, Hempel KA, Kypriamidis A. Appl Phys 1977;14:197.

[6] Sudakar C, Subbanna GN, Kutty TRN. J Magn Magn Mater 2003;263:253.

[7] Smit J, Lotgering FK, Enz U. J Appl Phys Suppl 1960;31:137 S.

[8] Albanese G, Carbicicchio M, Deriu A, Asti G, Rinaldi S. Appl Phys 1975;7:227.

[9] Obol M, Vittoria C. IEEE Trans Mag 2003;39:3103.

[10] Pullar RC, Bdikin IK, Bhattacharya AK. J Euro Ceram Soc 2012;32:905.

[11] Zhang C, Shi J, Yang X, De L, Wang X. Mater Chem Phys 2010;123:551.

[12] Verweel J. J Appl Phys 1967;38:1111.

[13] Jones GA. J Magn Magn Mater 1993;127:195.

[14] Jones GA, Parker SFH, Booth JG, Simkin DS. IEEE Trans Magn Magn 1990;26:2804.

[15] Perekalina TM, Shchvrova AD, Fonton SS, Annikov DG. Soviet Phys Jetp 1970;31:440.

[16] Castelliz LM, Kim KM, Boucher PS. J Can Ceram Soc 1969;38:57.

[17] Lee SG, Kwon SJ. J Magn Magn Mater 1996;153:279.

[18] Vaingankar AS, Kulkarni SG, Sagare MS. J Phys IV 1997;7:C1–155.

[19] G. Albanese, A. Deriu, F. Licci, S. Rinaldi, IEEE Trans. Magn. Magn 14 (1978) 710.

[20] A. Deriu, F. Licci, S. Rinaldi, T. Besagni, J. Magn. Magn. Mater. 22 (1981) 257.

[21] G.F.M. Pires Junior, et al. Journal of Alloys and Compounds (2010) 493:326-334

[22] Andrew Daigle, et al. J. Am. Ceram. Soc., 93 [10] 2994–2997 (2010).

[23] K. Komatsu, M. Nakanishi, T. Fujii, J. Takada, J. Magn. Magn. Mater. 272–276 (2004) e1831.

[24] J. Temuujin, M. Aoyama, M. Senna, T. Masuko, C. Ando, H. Kishi, J. Solid State Chem. 177 (2004) 3903.

[25] H.J. Zhang, X.L. Jia, X. Yao, L.Y. Zhang, J. Rare Earth 22 (2004) 338.

[26] Chunxiang Zhang, et al. Materials Chemistry and Physics (2010) 123:551-556.

[27] S. Bierlich, J. Topfer, J. Magn. Magn. Mater. (2012) 324:1804-1808.

[28] Y. Bai, W. Zhang, L. Qiao, Ji Zhou, J. Adv. Ceram. (2012) 1(2):100-109.